Two-Time Correlations of an Energy-Damped Bose-Einstein Condensate

Peter S. Barnett

September 2017

A dissertation submitted in partial fulfilment for
the degree of Bachelor of Science with Honours in Physics

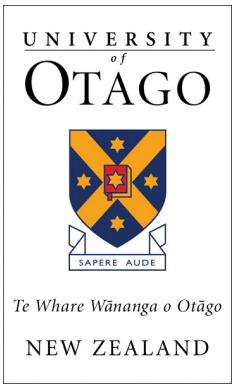

Abstract

Atomic Bose-Einstein condensates (BEC) are systems of interacting matterwaves that can exist in very low temperatures, demonstrating interesting nonlinear and finite temperature behaviour. The stochastic projected Gross-Pitaevskii equation (SPGPE) is used as a model for finite temperature BEC, by treating the low energy modes as a coherent region, and the high energy modes as a thermal reservoir. In this work we investigate the regime where particle exchange between these two regions is forbidden. This is achieved by having the two regions containing quantum mechanically distinguishable particles, a regime which occurs in the experimental technique of sympathetic cooling. Because the only allowed interactions between the two regions are number conserving, we are able to employ the energy-damped stochastic Gross-Pitaevskii equation.

The centre of mass motion of the condensate is found analytically to have the form of a damped harmonic oscillator subject to a random driving force. Analytic expressions for the damping and noise were found in terms of the system parameters.

These results were validated by finding analytical expressions for the two-time correlation functions of position and velocity for the damped harmonic oscillator with a random driving force, and comparing these with two-time correlation functions found using SPGPE simulations. Two physical regimes were investigated, one with a thermal cloud and condensate of ^{87}Rb , and one with a thermal cloud of ^{87}Rb and a condensate of ^{23}Na .

This comparison showed excellent agreement for low temperatures, as was expected because for our analytic results we had assumed the coherent region wavefunction had the form of the zero temperature Thomas-Fermi state. The higher temperature validity regime was investigated using the Penrose-Onsager criterion, and showed the expected divergence of the condensate wavefunction from the Thomas-Fermi state.

Acknowledgements

Firstly I would like to thank my supervisor Dr. Ashton Bradley for all of his immense help and support that he has given me this year. His positivity, enthusiasm, and advice are always appreciated, and without them this project would have been much more difficult, much less interesting, and probably unfinished.

I need to thank everyone in the Honours room this year, for the chats, the politics, and fellowship. Physics is so often a hard slog, and the company along the way makes it much more manageable, and sometimes even enjoyable.

I'd like to thank my parents, Alan and Ruth, for their endless love and support even if it is often in the form of smiles and nods to some nonsense rambling. I thank my sisters, Mary and Frances, out of obligation, but also for sometimes putting up with the boring physics talk.

And finally, I thank Celine, for keeping me alive this year, among all the other things.

Contents

Chapter 1

Introduction

Bose-Einstein condensation, was first achieved in a dilute alkali vapour in 1995 [1], and since then there has been significant experimental and theoretical work into the various properties and phenomena of these ultracold matterwaves. The Gross-Pitaevskii equation provides an excellent description of the zero temperature limit [2], describing all interactions in a single interacting condensate mode. The zero temperature limit is not physically attainable and we are forced to work at finite temperature, however at these temperatures the non-condensate fraction quickly becomes a significant feature of the system and as such, finite temperature theories must be employed, especially when approaching the critical temperature.

One finite temperature approach is the stochastic projected Gross-Pitaevskii equation [3], which treats the lower energy modes as a classical field, and the higher energy modes as a thermal reservoir. This theory takes into account the thermal interactions between the non-condensate and condensate regions. This theory includes both number-damping processes, in which the number of particles in the condensate changes, and energy-damping processes, where the number of particles is conserved, but energy is exchanged between the regions.

In this project we investigate the effects of energy-damping by considering a situation where number-damping processes are forbidden; where the thermal reservoir is a separate species to the low energy classical field. This is analogous to the sympathetic cooling regime, where a condensate is surrounded by an uncondensed thermal cloud with the aim of transferring energy between the two without the losses of particles that come from evaporative cooling [4].

We follow from the results of [5], and [6], in the regime where the condensate is pseudo-one dimensional, and the surrounding thermal cloud is three dimensional. Both of the components are contained in separate but overlapping harmonic potentials. An important theorem that can be applied to trapped interacting gases is the Kohn theorem, which states that the centre of mass motion will be independent of the interparticle interactions. Because of this, we expect the centre of mass motion of the condensate in a harmonic trap to undergo simple harmonic motion. This motion will be modified by the interactions with

the thermal component, resulting in damping and thermal noise.

The aims of this research are:

1. To find an analytical description for the centre of mass motion of the energy-damped, one dimensional condensate in a three dimensional thermal cloud. The analytical description of this quantum system will be understood by relating it to a simple classical model.
2. To find consistent physical parameters where our pseudo 1D model is valid while also being experimentally achievable.
3. To test our analytic results, by simulating the condensate numerically using the SPGPE with the physical parameters, and to find two-time correlation functions to compare with the classical model.

Chapter 2

Background

2.1 Bose-Einstein Condensation

Bose-Einstein condensation is a phenomena that may occur in a dilute gas of indistinguishable bosonic particles at very low temperature, in the order of 100 nK. This was first predicted by Einstein in 1924 based on the work of Bose on photon statistics. For an ideal non-interacting Bose gas at equilibrium the statistics can be described by the Bose-Einstein distribution[2],

$$n_{BE}(\epsilon) = \frac{1}{\mathrm{e}^{(\epsilon-\mu)/k_B T} - 1} \tag{2.1}$$

where $n_{BE}(\epsilon)$ is the number of particles with energy ϵ, in a system with chemical potential μ and temperature T. The chemical potential μ imposes a constraint on the number of particles in the system. Below a critical temperature T_c where μ approaches the lowest energy state, or in the ideal case μ approaches 0, a phase transition occurs resulting in macroscopic occupation of the ground state. At this temperature the de Broglie wavelength of an individual particle becomes comparable to the mean interparticle distance, this results in a coherent matter wave which is the Bose Einstein condensate.

Early evidence of BEC was in superfluid Helium, but the strong interparticle interactions stop the formation of a large condensate fraction. The first BEC achieved in an atomic gas was in 1995[1], using ^{87}Rb in a magnetic trap at 170 nK.

2.2 Zero Temperature Theory

2.2.1 Gross-Pitaevskii Equation

At zero temperature BEC is well described by the Gross-Pitaevskii Equation (GPE),

$$i\hbar\frac{\partial\psi(\mathbf{x},t)}{\partial t} = \left(-\frac{\hbar^2}{2m}\nabla^2 + V(\mathbf{x},t) + g|\psi(\mathbf{x},t)|^2\right)\psi(\mathbf{x},t) \tag{2.2}$$

where $V(\mathbf{x}, t)$ is the external potential. The variable g is the nonlinear interaction coefficient and characterises the interactions between the particles in the condensate. It is related to the s-wave scattering length, a_s, and mass, m, of the condensate particles by

$$g = \frac{4\pi a_s \hbar^2}{m}. \tag{2.3}$$

The GPE describes the dynamics of BEC well when the temperature is much less than the critical temperature. However when the temperature rises and the non-condensate fraction becomes more appreciable, the condensate, non-condensate and the interactions between the fractions play a significant role, and the GPE is not sufficient.

We can also define the time-independent GPE,

$$\mu\psi(\mathbf{x}) = \left(-\frac{\hbar^2}{2m}\nabla^2 + V(\mathbf{x}) + g|\psi(\mathbf{x})|^2\right)\psi(\mathbf{x}), \tag{2.4}$$

where μ is the chemical potential of the condensate.

2.2.2 Thomas-Fermi Approximation

A solution to the time-independent GPE at zero temperature is obtained by assuming the kinetic term is negligible, and choosing the wavefunction ansatz, $\Phi = \exp\left(-\frac{i\mu t}{\hbar}\right)\psi(\mathbf{x})$. For this ansatz the density is has no time dependence and only the phase evolves in time. Neglecting the kinetic energy terms is the essence of the Thomas-Fermi approximation. Substituting this into the GPE we obtain,

$$\mu \exp\left(-\frac{i\mu t}{\hbar}\right)\psi(\mathbf{x}) = \left(V(\mathbf{x}) + g|\psi(\mathbf{x})|^2\right)\exp\left(-\frac{i\mu t}{\hbar}\right)\psi(\mathbf{x}). \tag{2.5}$$

For $\psi(\mathbf{x}) \neq 0$ this can be solved for a region of the stationary Thomas-Fermi wavefunction, and for other regions we say $\psi(\mathbf{x}) = 0$, which is also consistent with our ansatz. This result can be written as

$$\psi_{TF}(\mathbf{x}) = \max\left[0, \sqrt{\frac{1}{g}\left(\mu - V(\mathbf{x})\right)}\right]. \tag{2.6}$$

In a 1D system with a harmonic potential $V(x) = \frac{1}{2}m\omega^2 x^2$, this becomes

$$\psi_{TF}(x) = \begin{cases} \sqrt{\frac{\mu}{g}\left(1 - \frac{x^2}{R^2}\right)} & |x| < R \\ 0 & |x| > R \end{cases} \tag{2.7}$$

where R is the Thomas-Fermi radius,

$$R = \sqrt{\frac{2\mu}{m\omega^2}}. \tag{2.8}$$

Hence the Thomas-Fermi density profile is an inverted parabola for $|x| < R$,

$$n_{TF}(x) = |\psi_{TF}(x)|^2 = n_0 \left(1 - \frac{x^2}{R^2}\right) \tag{2.9}$$

with peak density $n_0 = \mu/g$. This is a very good zero temperature approximation. For the wavefunction of condensate in a harmonic trap, the main difference is a smoothing out of the corners around $x = \pm R$ due to the kinetic energy contribution, Figure 2.1.

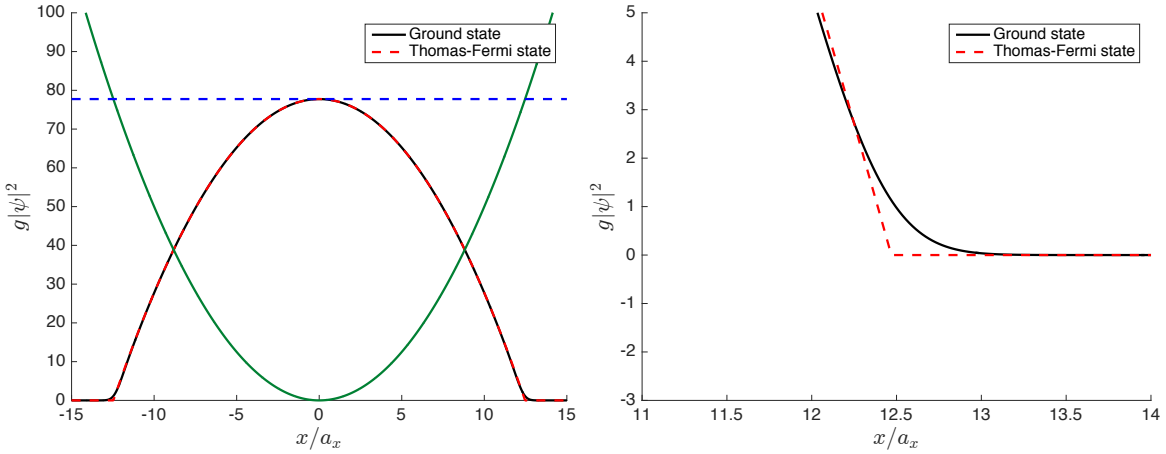

(a) **(b)**

Figure 2.1: Comparison of the Thomas-Fermi state with the real ground state. (a) The Thomas-Fermi State in red dashes, compared with the real ground state, the black line. The green line shows the harmonic trap potential, and the blue dashed line shows the system chemical potential, μ, in units of $\hbar\omega$. (b) The divergence at $x = +R$, showing how the ground state differs from the Thomas-Fermi at the edge of the condensate.

2.3 Kohn Mode Oscillations

The Kohn Theorem, was discovered in 1961 by W. Kohn, and states that the cyclotron resonance of an interacting electron gas is independent of the interparticle interactions[7]. This was later generalised to the case of an interacting harmonically trapped atomic gas by Dobson [8].

In the context of harmonically trapped BEC the Kohn theorem may be applied, leading to a mode of oscillation known as the Kohn mode. This form of oscillation is characterised by rigid sloshing of the density profile, with only the x-offset varying in time, and the shape of the condensate remaining constant. According to the Kohn theorem the centre of mass of an undamped system will oscillate at the characteristic frequency of the trap, regardless of any interparticle interactions. This oscillation will be described by simple harmonic motion [5].

2.4 Finite Temperature BEC

For zero temperature BEC, the GPE provides a very accurate model, as the system can be treated entirely as one coherent matter wave. For physical systems however, we are forced to work in finite temperature regimes. As the temperature increases, the number particles which are incoherent and form a thermal cloud will increase, and the population of the actual condensate will be reduced. These interactions between the incoherent regions and the condensate must be taken into account for an accurate model.

The interactions with the non-condensate region and the condensate will effect the Kohn mode oscillations in the form of thermal damping and driving. For this work we will use two important measures appropriate for describing finite temperature BEC. The first is two-time correlation functions of the condensate centre of mass (Section 5.2), which are involved in measuring the movement of the condensate and the effect of noise. We also use the Penrose-Onsager criterion for determining the occupation and spatial distribution of the condensate fraction (Section 6.2.2), this is important for finite temperatures as the condensate fraction decreases.

Chapter 3

C-field Formalism and the SPGPE

Here we give an outline of the C-field formalism used for describing finite temperature BEC and how it is used to give a formulation of the stochastic projected Gross-Pitaevskii equation (SPGPE). Here we are following the formulation originally from [9], as well as [10], [11] and [5].

For finite temperature BEC, the system is highly Bose degenerate with many highly occupied modes, and may be described as a classical field. C-field methods described shortly exploit this property and can be used to give accurate and physically interpretable descriptions.

3.1 Effective Field Theory

To understand the field description of BEC, we start with the second-quantised Hamiltonian for a Bose gas,

$$\hat{H} = \int d^3\mathbf{x}\hat{\Psi}^\dagger(\mathbf{x},t)\hat{H}_{sp}\hat{\Psi}(\mathbf{x},t) + \frac{1}{2}\int d^3\mathbf{x}\int d^3\mathbf{x}'\hat{\Psi}^\dagger(\mathbf{x},t)\hat{\Psi}^\dagger(\mathbf{x}',t)U(x-x')\hat{\Psi}(\mathbf{x}',t)\hat{\Psi}(\mathbf{x},t) \tag{3.1}$$

where $\hat{H}_{sp}$ is the single particle Hamiltonian,

$$\hat{H}_{sp} = \frac{\hbar^2}{2m}\nabla^2 + V(\mathbf{x},t). \tag{3.2}$$

Here as is in Section 2.2.1 $V(\mathbf{x},t)$ is the external potential. $\hat{\Psi}(\mathbf{x},t)$ and $\hat{\Psi}^\dagger(\mathbf{x},t)$ are the Bose field annihilation and creation operators respectively. $\hat{\Psi}(\mathbf{x},t)$ annihilates a particle at position $\mathbf{x}$ and time t, while $\hat{\Psi}^\dagger(\mathbf{x},t)$ creates a particle at position $\mathbf{x}$ and time t. These

operators have the standard Bosonic field commutation relations:

$$\left[\hat{\Psi}(\mathbf{x},t),\hat{\Psi}^{\dagger}(\mathbf{x}',t)\right]=\delta(\mathbf{x}-\mathbf{x}') \tag{3.3}$$

$$\left[\hat{\Psi}^{\dagger}(\mathbf{x},t),\hat{\Psi}^{\dagger}(\mathbf{x}',t)\right]=0 \tag{3.4}$$

$$\left[\hat{\Psi}(\mathbf{x},t),\hat{\Psi}(\mathbf{x}',t)\right]=0. \tag{3.5}$$

The interparticle interaction potential has a range determined by the effective size of the atoms, however because of the extremely low temperatures required for Bose-Einstein condensation, the atoms have very low thermal energy. Hence they have a thermal de Broglie wavelength greater than the interparticle interaction range. This allows us to ignore the effect of high momentum interactions. Formally this can be achieved by introducing an interparticle interaction of contact form,

$$U(\mathbf{x}-\mathbf{x}')=g\delta(\mathbf{x}-\mathbf{x}). \tag{3.6}$$

Here the strength of the interactions is characterised by the s-wave scattering length, as it is in the standard GPE, Equation 2.3. This description of the interactions is known as an *effective field theory*, and has the effective Hamiltonian

$$\hat{H}_{eff}=\int d^3\mathbf{x}\hat{\psi}^{\dagger}(\mathbf{x},t)\hat{H}_{sp}\hat{\psi}(\mathbf{x},t)+\frac{g}{2}\int d^3\mathbf{x}\hat{\psi}^{\dagger}(\mathbf{x},t)\hat{\psi}^{\dagger}(\mathbf{x},t)\hat{\psi}(\mathbf{x},t)\hat{\psi}(\mathbf{x},t). \tag{3.7}$$

This effective field theory is ultraviolet divergent, but this is resolved in the next section by introducing an energy cutoff for the field operator.

3.2 Projected Field Theory

Having already neglected the effect of high energy interactions by treating the interparticle interactions as a contact potential, we can divide the range of energies into two regions separated by an energy cutoff ϵ_{cut}. The **C** region , is the region below the new energy cutoff, $\epsilon_n \leq \epsilon_{cut}$, and has the highly occupied low energy modes, this allows us to treat it as partially coherent. The **I** region (**I** for incoherent) contains all the modes above this energy cutoff, $\epsilon_{cut} < \epsilon_n$, Figure 3.1. Modes in the **I** region of higher energy and so are expected to have occupation of order 1.

In this theory **C** is treated entirely quantum mechanically, while **I** is assumed to be fully thermalised.

To formally describe the **C** and **I** regions two projectors are defined; $\mathcal{P}$ projects into the **C** region neglecting modes above ϵ_{cut}, and $\mathcal{Q}$ projects into the **I** region, neglecting modes below ϵ_{cut}.

Tt is useful to express the projectors in the basis of single particle eigenstates, acting on an arbitrary object $F(\mathbf{x})$

$$\mathcal{P}\{F(\mathbf{x})\}=\sum_{n\in\mathbf{C}}\phi_n(\mathbf{x})\int d^3\mathbf{x}'\phi_n^*(\mathbf{x}')F(\mathbf{x}') \tag{3.8}$$

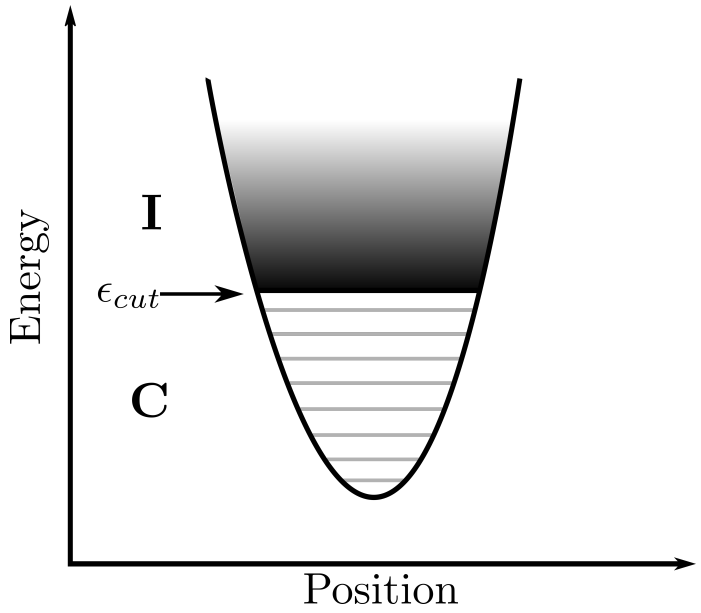

Figure 3.1: A schematic showing how the energy range is divided into the **C** and **I** regions, by introducing an energy cutoff ϵ_{cut}.

and

$$\mathcal{Q}\{F(\mathbf{x})\} = \sum_{n\in\mathbf{I}} \phi_n(\mathbf{x}) \int d^3\mathbf{x}' \phi_n^*(\mathbf{x}') F(\mathbf{x}'). \tag{3.9}$$

Hence the effective field operator can be expressed as,

$$\hat{\psi}(\mathbf{x},t) = \hat{\psi}_{\mathbf{C}}(\mathbf{x},t) + \hat{\psi}_{\mathbf{I}}(\mathbf{x},t) \tag{3.10}$$

where,

$$\mathcal{P}\left\{\hat{\psi}(\mathbf{x},t)\right\} = \hat{\psi}_{\mathbf{C}}(\mathbf{x},t) \tag{3.11}$$

and

$$\mathcal{Q}\left\{\hat{\psi}(\mathbf{x},t)\right\} = \hat{\psi}_{\mathbf{I}}(\mathbf{x},t). \tag{3.12}$$

Because **C** and **I** share no eigenmodes, the composition of a $\mathcal{P}$ and $\mathcal{Q}$ of any function is zero,

$$\mathcal{P}\{\mathcal{Q}\{F(x)\}\} = \mathcal{Q}\{\mathcal{P}\{F(x)\}\} = 0. \tag{3.13}$$

After projection into the **C** region, the commutation relations of $\hat{\psi}_{\mathbf{C}}(\mathbf{x},t)$ now use the course-grained, **C**-field delta function,

$$\left[\hat{\psi}_{\mathbf{C}}(\mathbf{x},t), \hat{\psi}^{\dagger}_{\mathbf{C}}(\mathbf{x}',t)\right] = \delta_{\mathbf{C}}(\mathbf{x},\mathbf{x}') \tag{3.14}$$

where

$$\delta_{\mathbf{C}}(\mathbf{x},\mathbf{x}') = \sum_{n\in\mathbf{C}} \phi_n(\mathbf{x},t)\phi_n^*(\mathbf{x}',t). \tag{3.15}$$

If this sum was not restricted to **C** then this would be a true Dirac delta function, however the **C**-field delta does have the same action when acting on function consisting of only modes in the **C** region. If $F(\mathbf{x}) = \mathcal{P}\{F(\mathbf{x})\}$, then

$$\int d^3\mathbf{x}' \delta_{\mathbf{C}}(\mathbf{x}, \mathbf{x}') F(\mathbf{x}') = F(\mathbf{x}). \tag{3.16}$$

3.3 Decomposition of the Effective Field Hamiltonian

The effective field Hamiltonian, Equation 3.7, can be decomposed using our projected field theory, giving the result,

$$\hat{H}_{eff} = \hat{H}_{\mathbf{C}} + \hat{H}_{\mathbf{I}} + \hat{H}_{\mathbf{C},\mathbf{I}} \tag{3.17}$$

where $\hat{H}_{\mathbf{C}}$ depends only on the **C**-field operator $\hat{\psi}_{\mathbf{C}}(\mathbf{x}, t)$, $\hat{H}_{\mathbf{I}}$ depends only on the **I**-field operator $\hat{\psi}_{\mathbf{I}}(\mathbf{x}, t)$, and $\hat{H}_{\mathbf{C},\mathbf{I}}$ depends on both the **C** and **I**-field operators. $\hat{H}_{\mathbf{C}}$ and $\hat{H}_{\mathbf{I}}$ are relatively simply expressed, and have the same form of $\hat{H}_{eff}$,

$$\hat{H}_{\mathbf{C}} = \int d^3\mathbf{x}\ \hat{\psi}^\dagger_{\mathbf{C}}(\mathbf{x}, t) \hat{H}_{sp} \hat{\psi}_{\mathbf{C}}(\mathbf{x}, t) + \frac{g}{2} \int d^3\mathbf{x} \hat{\psi}^\dagger_{\mathbf{C}}(\mathbf{x}, t) \hat{\psi}^\dagger_{\mathbf{C}}(\mathbf{x}, t) \hat{\psi}_{\mathbf{C}}(\mathbf{x}, t) \hat{\psi}_{\mathbf{C}}(\mathbf{x}, t) \tag{3.18}$$

$$\hat{H}_{\mathbf{I}} = \int\ d^3\mathbf{x} \hat{\psi}^\dagger_{\mathbf{I}}(\mathbf{x}, t) \hat{H}_{sp} \hat{\psi}_{\mathbf{I}}(\mathbf{x}, t) + \frac{g}{2} \int d^3\mathbf{x} \hat{\psi}^\dagger_{\mathbf{I}}(\mathbf{x}, t) \hat{\psi}^\dagger_{\mathbf{I}}(\mathbf{x}, t) \hat{\psi}_{\mathbf{I}}(\mathbf{x}, t) \hat{\psi}_{\mathbf{I}}(\mathbf{x}, t). \tag{3.19}$$

$\hat{H}_{\mathbf{C},\mathbf{I}}$ is the Hamiltonian for the interactions between the **C** and **I** regions, and can be split into three more terms,

$$\hat{H}_{\mathbf{C},\mathbf{I}} = \hat{H}^{(1)}_{\mathbf{C},\mathbf{I}} + \hat{H}^{(2)}_{\mathbf{C},\mathbf{I}} + \hat{H}^{(3)}_{\mathbf{C},\mathbf{I}} \tag{3.20}$$

where

$$\hat{H}^{(1)}_{\mathbf{C},\mathbf{I}} = g \int d^3\mathbf{x}\ \hat{\psi}^\dagger_{\mathbf{I}}(\mathbf{x}, t) \hat{\psi}^\dagger_{\mathbf{I}}(\mathbf{x}, t) \hat{\psi}_{\mathbf{I}}(\mathbf{x}, t) \hat{\psi}_{\mathbf{C}}(\mathbf{x}, t) + \text{h. c.} \tag{3.21}$$

$$\begin{aligned} \hat{H}^{(2)}_{\mathbf{C},\mathbf{I}} =& 2g \int d^3\mathbf{x}\ \hat{\psi}^\dagger_{\mathbf{I}}(\mathbf{x}, t) \hat{\psi}_{\mathbf{I}}(\mathbf{x}, t) \hat{\psi}^\dagger_{\mathbf{C}}(\mathbf{x}, t) \hat{\psi}_{\mathbf{C}}(\mathbf{x}, t) \\ &+ \frac{g}{2} \int\ d^3\mathbf{x} \hat{\psi}^\dagger_{\mathbf{I}}(\mathbf{x}, t) \hat{\psi}^\dagger_{\mathbf{I}}(\mathbf{x}, t) \hat{\psi}_{\mathbf{C}}(\mathbf{x}, t) \hat{\psi}_{\mathbf{C}}(\mathbf{x}, t) + \text{h. c.} \end{aligned} \tag{3.22}$$

$$\hat{H}^{(3)}_{\mathbf{C},\mathbf{I}} = g \int d^3\mathbf{x}\ \hat{\psi}^\dagger_{\mathbf{C}}(\mathbf{x}, t) \hat{\psi}^\dagger_{\mathbf{C}}(\mathbf{x}, t) \hat{\psi}_{\mathbf{C}}(\mathbf{x}, t) \hat{\psi}_{\mathbf{I}}(\mathbf{x}, t) + \text{h. c.} \tag{3.23}$$

where h. c. denotes the Hermitian conjugate. The terms involving $\hat{H}_{sp}$ and one $\hat{\psi}_{\mathbf{C}}$ and $\hat{\psi}_{\mathbf{I}}$ term each go to zero because the single particle modes in each region are orthogonal.

3.4 Wigner Formalism and Phase Space Methods

Phase space methods are an important tool for understanding and modelling BEC. For our **C**-field approach, all modes in the **C** region have significant occupation, which prompts us

to describe it using a classical field. In this case we express the state as a Wigner function, which is one of various representations of a state as a quasi-probability distribution in phase space[12].

3.4.1 Coherent States

Coherent states are very useful for describing BEC, and essential for the derivation of the SPGPE. These are a set of minimum uncertainty quantum states, and so their behaviour is closest to a classical description of any quantum state. Some systems display purely quantum phenomena, and cannot be described classically, but coherent states provide the closest description. A coherent state $|\alpha\rangle$, is an eigenstate of the annihilation operator, $\hat{a}$,

$$\hat{a}\,|\alpha\rangle = \alpha\,|\alpha\rangle \tag{3.24}$$

where α is a complex eigenvalue. These coherent states form an overcomplete basis and so any state can be expressed as a linear combination of them.

3.4.2 The Density Operator

A very useful way of describing a mixed state is as the density operator,

$$\hat{\rho}(t) = \sum_i p_i\,|\psi_i, t\rangle\,\langle\psi_i, t| \tag{3.25}$$

where $|\psi_i, t\rangle$ are the elements of the statistical ensemble that make up the mixed state and have the corresponding probability p_i. The density operator is an ideal description of quantum statistical ensembles because it accounts for both the statistical and quantum uncertainty of a system. The expectation value of an operator $\hat{A}$ for a system described by the density operator $\hat{\rho}$ is,

$$\langle\hat{A}\rangle = \mathrm{tr}\left\{\rho\hat{A}\right\}. \tag{3.26}$$

The time evolution of a system can be described by the time evolution of the density operator, which is found using the von Neumann equation,

$$i\hbar\frac{\partial\hat{\rho}}{\partial t} = \left[\hat{H}, \hat{\rho}\right]. \tag{3.27}$$

3.4.3 Wigner Function of a Single Mode

Phase space methods, such as the Wigner representation, rely on expressing the density operator in terms of α, the eigenvalue corresponding to the coherent state $|\alpha\rangle$. In the Wigner representation, this is done using the Wigner function[12],

$$W(\alpha, \alpha^*) = \frac{1}{\pi^2}\int d^2\lambda \exp[-\lambda\alpha^* + \lambda^*\alpha]\chi(\lambda, \lambda^*) \tag{3.28}$$

which is the Fourier transform of the symmetrically ordered characteristic function,

$$\chi(\lambda, \lambda^*) = \mathrm{tr}\left\{\hat{\rho}\exp\left[\lambda\hat{a}^\dagger - \lambda^*\hat{a}\right]\right\}. \tag{3.29}$$

Because α and α^* are complex conjugates, they have two degrees of freedom between them, and can be treated as independent variables.

For any density operator, we are able to define a Wigner function. There exist mappings from creation and annihilation operators acting on the density operator to equivalent forms of differential operators acting on the corresponding Wigner function:

$$\hat{a}\hat{\rho} \longleftrightarrow \left(\alpha + \frac{1}{2}\frac{\partial}{\partial\alpha^*}\right) W(\alpha, \alpha^*) \tag{3.30}$$

$$\hat{a}^\dagger\hat{\rho} \longleftrightarrow \left(\alpha^* - \frac{1}{2}\frac{\partial}{\partial\alpha}\right) W(\alpha, \alpha^*) \tag{3.31}$$

$$\hat{\rho}\hat{a} \longleftrightarrow \left(\alpha - \frac{1}{2}\frac{\partial}{\partial\alpha^*}\right) W(\alpha, \alpha^*) \tag{3.32}$$

$$\hat{\rho}\hat{a}^\dagger \longleftrightarrow \left(\alpha^* + \frac{1}{2}\frac{\partial}{\partial\alpha}\right) W(\alpha, \alpha^*) \tag{3.33}$$

These mapping relations can be used to go from the density matrix, to the evolution of the Wigner function.

3.4.4 Generalisation to a Quantum Field

These mappings from the density matrix to the Wigner function can be generalised to the action of quantum field operators on the density matrix using expansion of the field operator in terms of creation and annihilation operators,

$$\hat{\psi}_{\mathbf{C}}(\mathbf{x}) = \sum_{n\in\mathbf{C}} \hat{a}_n\phi_n(\mathbf{x}). \tag{3.34}$$

Using the definition of projected functional derivatives[10, 11],

$$\frac{\bar{\delta}}{\bar{\delta}\psi_{\mathbf{C}}(\mathbf{x})} \equiv \sum_{n\in\mathbf{C}} \phi_n^*(\mathbf{x})\frac{\partial}{\partial\alpha_n} \tag{3.35}$$

$$\frac{\bar{\delta}}{\bar{\delta}\psi^*_{\mathbf{C}}(\mathbf{x})} \equiv \sum_{n\in\mathbf{C}} \phi_n(\mathbf{x})\frac{\partial}{\partial\alpha_n^*}, \tag{3.36}$$

the mappings from the action of the field operators on the density matrix to the action of projected functional differential operators on the Wigner function are:

$$\hat{\psi}_{\mathbf{C}}(\mathbf{x})\hat{\rho}_{\mathbf{C}} \longleftrightarrow \left(\psi_{\mathbf{C}}(\mathbf{x}) + \frac{1}{2}\frac{\bar{\delta}}{\bar{\delta}\psi^*_{\mathbf{C}}(\mathbf{x})}\right) W_{\mathbf{C}} \tag{3.37}$$

$$\hat{\psi}^\dagger_{\mathbf{C}}(\mathbf{x})\hat{\rho}_{\mathbf{C}} \longleftrightarrow \left(\psi^*_{\mathbf{C}}(\mathbf{x}) - \frac{1}{2}\frac{\bar{\delta}}{\bar{\delta}\psi_{\mathbf{C}}(\mathbf{x})}\right) W_{\mathbf{C}} \tag{3.38}$$

$$\hat{\rho}_{\mathbf{C}}\hat{\psi}_{\mathbf{C}}(\mathbf{x}) \longleftrightarrow \left(\psi_{\mathbf{C}}(\mathbf{x}) - \frac{1}{2}\frac{\bar{\delta}}{\bar{\delta}\psi^*_{\mathbf{C}}(\mathbf{x})}\right) W_{\mathbf{C}} \tag{3.39}$$

$$\hat{\rho}_{\mathbf{C}}\hat{\psi}^\dagger_{\mathbf{C}}(\mathbf{x}) \longleftrightarrow \left(\psi^*_{\mathbf{C}}(\mathbf{x}) + \frac{1}{2}\frac{\bar{\delta}}{\bar{\delta}\psi_{\mathbf{C}}(\mathbf{x})}\right) W_{\mathbf{C}} \tag{3.40}$$

We can used these mappings to relate the coherent region density operator to the time evolution of the Wigner function.

3.5 The Stochastic Projected Gross-Pitaevskii Equation

The evolution of the full system is governed by the von Neumann equation,

$$i\hbar\frac{\partial}{\partial t}\hat{\rho} = \left[\hat{H}_{\mathbf{C}} + \hat{H}_{\mathbf{I}} + \hat{H}_{\mathbf{C},\mathbf{I}}, \hat{\rho}\right]. \tag{3.41}$$

We are able to find the master equation for just the **C** region by defining the **C** region density operator,

$$\hat{\rho}_{\mathbf{C}} \equiv \mathrm{tr}_{\mathbf{I}}\{\hat{\rho}\}, \tag{3.42}$$

which eliminates the degrees of freedom of the **I** region. This is possible as the **C** and **I** regions are uncorrelated ans thus the density operators for the two regions are separable. This results in the master equation for the **C** region,

$$\frac{\partial\hat{\rho}_{\mathbf{C}}}{\partial t} = \left.\frac{\partial\hat{\rho}_{\mathbf{C}}}{\partial t}\right|_H + \left.\frac{\partial\hat{\rho}_{\mathbf{C}}}{\partial t}\right|_\gamma + \left.\frac{\partial\hat{\rho}_{\mathbf{C}}}{\partial t}\right|_\epsilon. \tag{3.43}$$

Using the mappings Equations 3.37–3.40, after applying the truncated Wigner approximation by ignoring the effect of third order functional derivatives, this master equation can be mapped to an Fokker-Planck equation [13, 12]. This Fokker-Planck equation is subsequently mapped to a stochastic differential equation, the SPGPE, with three terms, corresponding to the terms in Equation 3.43[3].

The first term in the SPGPE (Equation 3.43) is simple Hamiltonian evolution for the **C** region, without the effect of interactions with the **I** region, and can be expressed as,

$$d\psi_{\mathbf{C}}|_H\, \mathcal{P}\left\{-\frac{i}{\hbar}L_{\mathbf{C}}\psi_{\mathbf{C}}(\mathbf{x},t)dt\right\} \tag{3.44}$$

where,

$$L_{\mathbf{C}} = -\frac{\hbar^2}{2m}\nabla^2 + V(\mathbf{x},t) + g|\psi_{\mathbf{C}}(\mathbf{x},t)|^2. \tag{3.45}$$

The second term is responsible for number-damping and involves processes where the interactions between the **C** and **I** regions do not conserve particle number (Figure 3.2a). Generally this is the dominant interaction between the two regions and it's properties have been investigated in other research[14, 15]. For this regime however, because the condensate is surrounded by a cloud of distinct atoms, this term is ignored, which is discussed more in Section 4.2.1 .

(a) Number-damping **(b)** Energy-damping

Figure 3.2: From [5]. Schematic showing the different interactions between the **C** and **I** regions. (a) A number-damping process, whereby the number of particles in each region is not conserved. (b) An energy-damping process where the number of particles in each region is unchanged, but there is transfer of energy.

The third term is the energy-damping term, and corresponds to processes where there is an exchange of energy between the **C** and **I** regions, but the particle number is conserved (Figure 3.2b). These processes are also referred to as scattering processes. It may be expressed as,

$$d\psi_{\mathbf{C}}|_{\epsilon} = \mathcal{P}\left\{-\frac{i}{\hbar}V_{\epsilon}(\mathbf{x},t)\psi_{\mathbf{C}}(\mathbf{x},t)dt + i\psi_{\mathbf{C}}(\mathbf{x},t)dW_{\epsilon}(\mathbf{x},t)\right\}. \tag{3.46}$$

$V_{\epsilon}(\mathbf{x},t)$ can be interpreted as an energy-damping potential and has the form

$$V_{\epsilon}(\mathbf{x},t) = -\hbar\int d^3\mathbf{x}'\epsilon(\mathbf{x}-\mathbf{x}')\nabla'\cdot\mathbf{j}(\mathbf{x}',t) \tag{3.47}$$

with the **C**-field density current is,

$$\mathbf{j}(\mathbf{x},t) = \frac{i\hbar}{2m}[\psi_{\mathbf{C}}(\mathbf{x},t)\nabla\psi^*_{\mathbf{C}}(\mathbf{x},t) - \psi^*_{\mathbf{C}}(\mathbf{x},t)\nabla\psi_{\mathbf{C}}(\mathbf{x},t)]. \tag{3.48}$$

$\epsilon(\mathbf{x})$ is defined as the Fourier transform of the scattering kernel,$S(k)$, with a factor of the energy damping rate,

$$\epsilon(\mathbf{x}) = \frac{\mathcal{M}}{(2\pi)^3}\int d^3\mathbf{k}\, e^{i\mathbf{k}\cdot\mathbf{x}}\, S(\mathbf{k}) \tag{3.49}$$

where the energy damping rate for indistinguishable particles is,

$$\mathcal{M} = \frac{16\pi a_s^2}{e^{(\epsilon_{cut}-\mu)/k_BT}-1}. \tag{3.50}$$

The noise term in the energy-damping term is defined by its correlations,

$$\overline{dW_\epsilon(\mathbf{x},t)dW_\epsilon(\mathbf{x}',t)} = \frac{2k_BT}{\hbar}\epsilon(\mathbf{x}-\mathbf{x}')dt, \tag{3.51}$$

where $\overline{\cdots}$ represents the average over many different realisations. This noise is real, and due to the $\epsilon(\mathbf{x}-\mathbf{x}')$ term in the correlator, is non-local in position. It appears in the SPGPE multiplied by the wavefunction, so is multiplicative. This makes it much more difficult to deal with numerically compared to additive noise, such as is part of the number-damping term.

Chapter 4

Physical Regime

The specific regime being investigated in this work is a two component system; a pseudo-1D condensate (component 1) surrounded by a thermal cloud of a distinct species (component 2) (Figure 4.1). For this research the components are treated as bosonic. This regime is analogous to a sympathetic cooling regime, which is used experimentally to cool condensates via exchange of energy with an uncondensed thermal cloud. In this regime, the condensate and the thermal cloud are confined in two separate, but spatially overlapping traps.

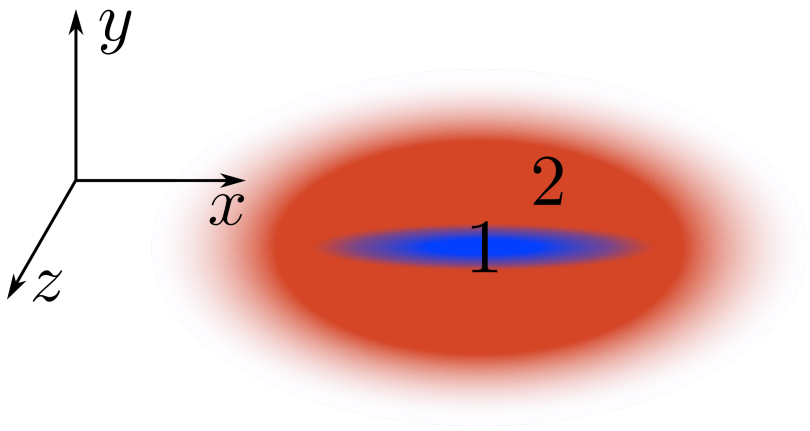

Figure 4.1: A schematic demonstrating the pseudo-1D partially condensed component 1 in the 3D thermal cloud of component 2.

4.1 Use of C-field Methods

C-field theory provides a useful way to model this two-component system. At low temperatures component 1, the condensate, will have a high condensate fraction and low occupation of higher energy modes. Treating the higher energy levels as having negligible occupation

prompts us to define an energy cutoff for the condensate, $\epsilon_{cut,1}$, such that all occupied modes are in the **C** region. For an effective 1D system there must be no excitations of the transverse modes of the condensate. For high enough transverse frequencies, we can choose the energy cutoff of the condensate to be lower than energy of the first excited transverse mode. Because modes above this cutoff are neglected, the transverse excitations are effectively frozen out, and the system can be treated as 1 dimensional.

Conversely, the thermal cloud has a negligible condensate fraction and so we can treat all modes as being in the **I** region. Treating all of the modes as being in the **I** region is equivalent to defining an energy cutoff for the second component, $\epsilon_{cut,2}$, and taking it to zero, $\epsilon_{cut,2} \to 0$. This evidently leaves no modes in the **C** region for component 2.

This differs from the standard **C**-field treatment of a finite temperature BEC where both the **C** and **I** regions are of the same species, and **I** just represents the uncondensed fraction. In this regime, the **C** and **I** regions are made up from separate but interacting species. Component 2 still behaves like the **I** region, and can be treated as a thermal reservoir. However because the two components are composed of different species, no particle exchange between the **C** and **I** regions is allowed, and the only transfer of energy is via scattering interactions.

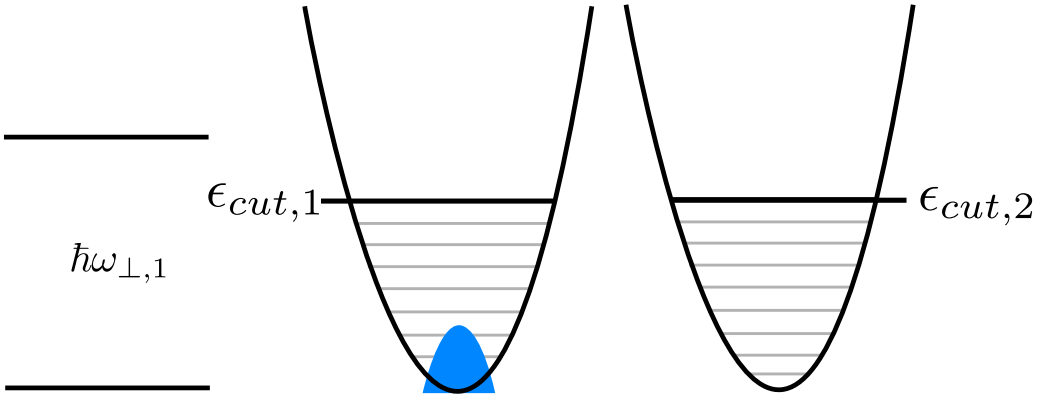

Figure 4.2: Schematic showing the use of **C** field methods for describing this two component system. The energy cutoff, $\epsilon_{cut,1}$, is chosen such that transverse oscillations in component 1 are forbidden. Component 1 is treated as having only appreciable occupation in the **C** region, while component 2 is treated as being entirely incoherent.

4.2 One Dimensional Energy Damped SPGPE

4.2.1 Energy Damping

Because the **C** and **I** regions are assumed to be of separate species, only number conserving interactions are allowed. The number of particles in each component is constant, and all interactions between the two regions will only transfer energy. This prompts the simplification of the SPGPE, by removing the number damping term, resulting in the energy

damped SPGPE,

$$(S)d\psi_{\mathbf{C}}(\mathbf{x},t) = \mathcal{P}\left\{-\frac{i}{\hbar}L_{\mathbf{C}}\psi_{\mathbf{C}}(\mathbf{x},t)dt - \frac{i}{\hbar}V_{\epsilon}(\mathbf{x},t)\psi_{\mathbf{C}}(\mathbf{x},t)dt + i\psi_{\mathbf{C}}(\mathbf{x},t)dW_{\epsilon}(\mathbf{x},t)\right\}. \quad (4.1)$$

This equation has the standard Hamiltonian evolution given by $L_{\mathbf{C}}$ (Equation 3.45), and also time evolution due to the energy damping potential, $V_{\epsilon}(\mathbf{x},t)$ and the noise associated with the energy damping processes, $dW_{\epsilon}(\mathbf{x},t)$.

4.2.2 Reduced Dimensionality

To be able to treat the condensate as a one dimensional system we have to make adjustments to the SPGPE to remove the dependence on the transverse directions. This is done by integrating over the transverse directions, where the condensate is in the unexcited state and is assumed to be Gaussian. Here we use results from [10] and [16]. Transforming the energy damped SPGPE (Equation 4.1) into one dimension, we obtain,

$$(S)d\psi_{\mathbf{C}}(x,t) = \mathcal{P}\left\{-\frac{i}{\hbar}L_{\mathbf{C}}\psi_{\mathbf{C}}(x,t)dt - \frac{i}{\hbar}V_{\epsilon}(x,t)\psi_{\mathbf{C}}(x,t)dt + i\psi_{\mathbf{C}}(x,t)dW_{\epsilon}(x,t)\right\}. \quad (4.2)$$

All of the terms here are now the one dimensional equivalents,

$$L_{\mathbf{C}}\psi_{\mathbf{C}}(x,t) = \left(-\frac{\hbar^2}{2m}\frac{\partial^2}{\partial x^2} + V(x) + g_1|\psi_{\mathbf{C}}(x,t)|^2\right)\psi_{\mathbf{C}}(x,t) \quad (4.3)$$

where $g_1 = 2\hbar\omega_{\perp,1}a_{11}$ is the one dimensional form of the non-linear interaction coefficient, obtained by integrating non-linear interaction term of the full GPE over the transverse directions.

The energy damping potential in one dimension is given by,

$$V_{\epsilon}(x,t) = -\hbar\int dx'\epsilon(x-x')\frac{\partial}{\partial x'}j(x',t), \quad (4.4)$$

where $j(x,t)$ is the one dimensional current density,

$$j(x,t) = \frac{i\hbar}{2m}\left[\psi_{\mathbf{C}}(x,t)\frac{\partial}{\partial x}\psi^*_{\mathbf{C}}(x,t) - \psi^*_{\mathbf{C}}(x,t)\frac{\partial}{\partial x}\psi_{\mathbf{C}}(x,t)\right]. \quad (4.5)$$

$\epsilon(x)$ is now the energy damping rate multiplied by the Fourier transform of the scattering kernel, both of which have distinct one dimensional forms,

$$\epsilon(x) = \frac{\mathcal{M}}{2\pi}\int dk\, \mathrm{e}^{ikx}\, S_1(k) \quad (4.6)$$

where the one dimensional form of the energy damping rate which is modified to take into account for component 1 and component 2 consisting of distinct particles, and after taking $\epsilon_{cut,2} \to 0$ is,

$$\mathcal{M} = \frac{8\pi a_{12}^2}{\mathrm{e}^{-\mu_2/k_BT} - 1} \quad (4.7)$$

and the one dimensional scattering kernel is,

$$S_1(k) = \frac{1}{\sqrt{8\pi a_{\perp,1}^2}} \operatorname{erfcx}\left(\frac{a_{\perp,1}|k|}{\sqrt{2}}\right) \tag{4.8}$$

where $\operatorname{erfcx}(x) = \exp(x^2)\operatorname{erfc}(x)$ is the scaled complementary error function. The noise associated with the energy damping in one dimension has correlations in position defined by,

$$\overline{dW_\epsilon(x,t)dW_\epsilon(x',t)} = \frac{2k_BT}{\hbar}\epsilon(x-x')dt. \tag{4.9}$$

4.3 Choice of Physical Parameters

Here we discuss the restrictions on the physical parameters such that our regime is leads to a physically valid theory. There are several parameters that describe the two components, and these must be chosen such that we are within the desired physical regime. We chose the temperature of the system such that we are in the correct thermal regime, where component 1 is partially condensed and component 2 can be treated as a thermal cloud. The geometry of the traps must allow us to be in the correct dimensional regime. Our choices of temperature and trap geometry must also be physically consistent with the component populations and chemical potentials. For this work the principle frequency for analytic and numeric investigation is the loose component 1 frequency, $\omega_{x,1}$, so we define,

$$\Omega = \omega_{x,1}. \tag{4.10}$$

4.3.1 Temperature Regime

The physical regime that is being investigated imposes several restrictions on the choice of parameters. The temperature of the system, which is the same in each component, must be in the range where component 2 is thermalised, and component 1 has a large enough condensate fraction such that it is well described by the Thomas-Fermi state. Broadly the temperature must be greater than $T_{c,2}$ and less than $T_{c,1}$,

$$T_{c,2} < T \lesssim T_{c,1} \tag{4.11}$$

although more restrictions are also imposed.

Component 2, a thermal cloud, can be reasonably treated as a 3D ideal gas, with critical temperature given by [2]

$$T_{c,2} = \frac{\hbar\bar{\omega}_2}{k_B}\left(\frac{N_2}{\zeta(3)}\right)^{1/3}, \tag{4.12}$$

where N_2 is the population of component 2, $\bar{\omega_2}$ is the geometric mean trapping frequency of component 2,

$$\bar{\omega_2} = (\omega_{x,2}\ \omega_{y,2}\ \omega_{z,2})^{1/3} = \left(\omega_{x,2}\ \omega_{\perp,2}^2\right)^{1/3}. \tag{4.13}$$

Because component 1 is confined to a one-dimensional subspace of a harmonic trap, deeper analysis is required to find the critical temperature. We can find a reasonable approximation for critical temperature for component 1 by ignoring the interaction effects [17], and numerically solving

$$N_1 = \frac{k_B T_{c,1}}{\hbar\Omega} \ln\left(\frac{2k_B T_{c,1}}{\hbar\Omega}\right), \tag{4.14}$$

this corresponds to all of the particles in component 1 being excited above the ground state. Under these same approximations, the condensate fraction of component 1 is given by

$$\frac{N_{1,0}}{N_1} = 1 - \frac{T \ln\left(2k_B T/(\hbar\Omega)\right)}{T_{c,1} \ln\left(2k_B T_{c,1}/(\hbar\Omega)\right)} \tag{4.15}$$

where N_1 is the total population of component 1 and $N_{1,0}$ is the population of component 1 in the ground state. For the validity of our analytical approach, the condensate fraction must be high enough such that the wavefunction is still approximately Thomas-Fermi, so that this can be used as an analytical ansatz.

For our 2 component system, the number of particles in each component is conserved independently, and so the number of particles in each of the components sets the respective chemical potential for each component.

4.3.2 Trapping Geometry

As stated before, for component 1 to be treated as one dimensional no particles can be excited in the transverse direction. This can be achieved by setting the chemical potential less than the energy of the first transverse excited state,

$$\mu_1 < \hbar\omega_{\perp,1}. \tag{4.16}$$

This means that the energy of component 1 is less than what would be required to excite the condensate in the transverse direction.

At the same time, we must also make sure that the condensate is not too squeezed in the transverse direction, because our model relies on 3D scattering within the condensate. This can be ensured by making sure that the harmonic transverse oscillator length, $a_{\perp,1}$, is much greater than the s-wave scattering length,

$$\sqrt{\frac{\hbar}{m_1\omega_{\perp,1}}} = a_{\perp,1} \gg a_{11}. \tag{4.17}$$

Because component 2 is modelled as an ideal gas, there are few restrictions placed on the trap geometry. This allows us change $\omega_{x,2}$ and $\omega_{\perp,2}$ while still being in the desired regime.

Chapter 5

Analytical Results

In this section we start by performing a revised and generalised derivation for the condensate equation of motion from a previous work [5].

5.1 Condensate Centre of Mass Motion

5.1.1 Centre of Mass of a Multiparticle Wavefunction

Because the condensate is described by a multiparticle wavefunction of N_1 particles of mass m, the wavefunction is normalised to N_1

$$\int |\psi|^2 dx = N_1. \tag{5.1}$$

The expectation value of the position of the centre of mass, X, can be found by

$$X = \frac{\langle \hat{x} \rangle}{N_1} = \frac{1}{N_1} \int \psi^* \hat{x} \psi dx \tag{5.2}$$

where $\hat{x}$ is the single particle position operator. Similarly, the velocity of the centre of mass of the condensate can be found by

$$V = \frac{\langle \hat{p} \rangle}{N_1 m} = \frac{1}{N_1 m} \int \psi^* \hat{p} \psi dx \tag{5.3}$$

where $\hat{p}$ is the single particle momentum operator

$$\hat{p} = -i\hbar \frac{\partial}{\partial x}. \tag{5.4}$$

It is assumed that the wavefunction remains approximately as a Thomas-Fermi wavefunction with an position offset, which we can use as an ansatz for this analytical work

$$\psi_{TF}(x,t) = \sqrt{\frac{\mu}{g_1}\left(1 - \frac{(x - X(t))^2}{R^2}\right)}\, \mathrm{e}^{iP(t)x/\hbar}. \tag{5.5}$$

This has the density profile:

$$n_{TF}(x,t) \equiv |\psi_{TF}(x,t)|^2 = n_0 \left(1 - \frac{(x - X(t))^2}{R^2}\right) \tag{5.6}$$

where n_0 is the peak density, R is the 1D Thomas-Fermi radius, and g_1 is the 1D interaction parameter

$$n_0 = \frac{\mu}{g_1}, \qquad R = \sqrt{\frac{2\mu}{m\Omega^2}} \qquad g_1 = 2\hbar\omega_{\perp,1}a_1. \tag{5.7}$$

The total number of particles in a Thomas-Fermi state is found by

$$N_1 = \int_{X(t)-R}^{X(t)+R} n_{TF}(x,t)dx = \int_{X(t)-R}^{X(t)+R} dx\ n_0 \left(1 - \frac{(x - X(t))^2}{R^2}\right). \tag{5.8}$$

$$\tag{5.9}$$

Thus,

$$N_1 = \frac{4\mu R}{3g_1}. \tag{5.10}$$

It is also useful to evaluate the 1D current density for the Thomas-Fermi state:

$$j(x,t) = \frac{i\hbar}{2m}\left[\psi(x,t)\frac{\partial}{\partial x}\psi^*(x,t) - \psi^*(x,t)\frac{\partial}{\partial x}\psi(x,t)\right]. \tag{5.11}$$

For $\psi(x,t) = \psi_{TF}(x,t)$,

$$\psi(x,t)\frac{\partial}{\partial x}\psi^*(x,t) = -\frac{\mu}{g_1}\frac{(x - X(t))}{R^2} + \frac{-iP(t)}{\hbar}\frac{\mu}{g_1}\left(1 - \frac{(x - X(t))}{R^2}\right) \tag{5.12}$$

$$= -\frac{\mu}{g_1}\frac{(x - X(t))}{R^2} + \frac{-iP(t)}{\hbar}n_{TF}(x,t). \tag{5.13}$$

And so,

$$j(x,t) = \frac{i\hbar}{2m}\left[\frac{-iP(t)}{\hbar}n_{TF}(x,t) - \frac{+iP(t)}{\hbar}n_{TF}(x,t)\right] = \frac{P(t)}{m}n_{TF}(x,t). \tag{5.14}$$

Thus giving us the expression for current density,

$$j(x,t) = n_{TF}(x,t)V(t). \tag{5.15}$$

5.1.2 Derivation of Equation of Motion

Following the results of [6] and [5], starting from the equation for the field momentum

$$P(\psi,\psi^*) = \int dx\ \psi^*(x,t)\left(-i\hbar\frac{\partial}{\partial x}\right)\psi(x,t) \tag{5.16}$$

we apply a change of variables using the Ito rules[13], and evaluate the functional derivatives of $P(\psi^*, \psi)$. This leads to a Langevin equation for the field momentum:

$$dP(t) = F(t)dt + \sqrt{G(t)}dW(t) \tag{5.17}$$

where

$$F(t) = -\int dx n_{TF}(x,t)\frac{\partial}{\partial x}V_{ext} + F_\epsilon(x,t) \tag{5.18}$$

$$G(t) = 2\hbar k_B T \int dx \int dx' \epsilon(x-x')\frac{\partial}{\partial x}n_{TF}(x,t)\frac{\partial}{\partial x'}n_{TF}(x',t), \tag{5.19}$$

and the noise term $dW(t)$ is a real Wiener process defined with, $\overline{dW(t) = 0}$ and $\overline{dW(t)dW(t)} = dt$[6].

$F(t)$ has two terms that can be evaluated separately; the first term which depends on the external potential $V_{ext}(x)$, and $F_\epsilon(x,t)$ which depends on an effective energy damping potential $V_\epsilon(x,t)$.

The external potential is $V_{ext} = \frac{1}{2}m\Omega^2 x^2$ so $\frac{\partial}{\partial x}V_{ext} = m\Omega^2 x$,

$$-\int dx n_{TF}(x,t)\frac{\partial}{\partial x}V_{ext} = -\int dx |\psi|^2 m\Omega^2 x \tag{5.20}$$

$$= -\Omega^2 m N_1 X. \tag{5.21}$$

For the second term[16],

$$F_\epsilon(t) = -\int dx\ n_{TF}(x,t)\frac{\partial}{\partial x}V_\epsilon(x,t). \tag{5.22}$$

We have the form of $V_\epsilon(x,t)$, and can apply integration by parts

$$V_\epsilon(x,t) = -\hbar\int dx'\epsilon(x-x')\frac{\partial}{\partial x'}j(x',t) \tag{5.23}$$

$$= -\hbar\epsilon(x-x')j(x',t)|_{X-R}^{X+R} + \hbar\int dx'\frac{\partial}{\partial x'}\epsilon(x-x')j(x',t). \tag{5.24}$$

The first term is equal to zero because there is no density at $x = X \pm R$, so the current density, $j(x,t)$, also goes to zero here. Thus,

$$V_\epsilon(x,t) = \hbar\int dx'\frac{\partial}{\partial x'}\epsilon(x-x')j(x',t). \tag{5.25}$$

We know $\epsilon(x)$ (Equation 4.6) is the inverse Fourier transform of the scattering kernel $S_1(k)$ [18, 16] so,

$$\frac{\partial}{\partial x'}\epsilon(x-x') = \frac{\mathcal{M}}{2\pi}\int_{-\infty}^{\infty} dk(-ik)\,\mathrm{e}^{ik(x-x')}\,S_1(k). \tag{5.26}$$

We can now use Equations 5.25 and 5.26 to find $\frac{\partial}{\partial x}V_\epsilon(x,t)$ for Equation 5.22

$$\frac{\partial}{\partial x}V_\epsilon(x,t) = \frac{\hbar\mathcal{M}}{2\pi}\int dx' \int_\infty^\infty dk\ k^2\, \mathrm{e}^{ik(x-x')}\, S_1(k) n_{TF}(x,t)V(t). \tag{5.27}$$

So $F_\epsilon(x,t)$ can be evaluated as, using 5.25,

$$\begin{aligned} F_\epsilon(t) =& -\int dx\ n_{TF}(x,t)\frac{\partial}{\partial x}V_\epsilon(x,t) && (5.28)\\ =& -V(t)\frac{\hbar\mathcal{M}}{2\pi}\int dk\ S_1(k)\ k^2\left[\left(\int dx\ n_{TF}(x,t)\,\mathrm{e}^{ikx}\right)\left(\int dx'\ n_{TF}(x',t)\,\mathrm{e}^{-ikx'}\right)\right]. && (5.29)\end{aligned}$$

We will now evaluate $G(t)$ using integration by parts, remembering that $n_{TF}(x,t) = 0$ for $x \notin [X-R,\ X+R]$

$$\begin{aligned} G(t) =& 2\hbar k_B T\int dx\int dx' \epsilon(x-x')\frac{\partial}{\partial x}n_{TF}(x,t)\frac{\partial}{\partial x'}n_{TF}(x',t)\\ =& 2\hbar k_B T\left[n_{TF}(x,t)\int dx'\ \epsilon(x-x')\frac{\partial}{\partial x'}n_{TF}(x',t)\right]_{x=-\infty}^{x=\infty}\\ & -2\hbar k_B T\int dx\ n_{TF}(x,t)\frac{\partial}{\partial x}\left[\int dx'\epsilon(x-x')\frac{\partial}{\partial x'}n_{TF}(x',t)\right]. \end{aligned}$$

The first term in the second equation goes to zero and by applying the same method again, we arrive at

$$\begin{aligned} G(t) =& 2\hbar k_B T\int dx\int dx'\ n_{TF}(x,t)\ n_{TF}(x',t)\frac{\partial}{\partial x}\frac{\partial}{\partial x'}\epsilon(x-x') && (5.30)\\ =& \frac{\mathcal{M}\hbar k_B T}{\pi}\int dk\ S_1(k)\ k^2\left[\left(\int dx\ n_{TF}(x,t)\,\mathrm{e}^{ikx}\right)\left(\int dx'\ n_{TF}(x',t)\,\mathrm{e}^{-ikx'}\right)\right]. && (5.31)\end{aligned}$$

The integral terms in $G(t)$ and $F_\epsilon(t)$ (Equations 5.31 and 5.29), are the same. This integral is computed in Appendix A.

Using the form of $S_1(k)$

$$S_1(k) = \frac{1}{\sqrt{8\pi a_\perp^2}}\,\mathrm{erfcx}\left(\frac{|k|a_\perp}{\sqrt{2}}\right), \tag{5.32}$$

$$\begin{aligned} &\int dk\ S_1(k)\ k^2\left[\left(\int dx\ n_{TF}(x,t)\,\mathrm{e}^{ikx}\right)\left(\int dx'\ n_{TF}(x',t)\,\mathrm{e}^{-ikx'}\right)\right] =\\ &\qquad\frac{32n_0^2}{R\sqrt{8\pi a_\perp^2}}\int_0^\infty dz\,\mathrm{erfcx}\left(\frac{\lambda z}{\sqrt{2}}\right)\ z^2\left(\frac{\cos(z)}{z^2}-\frac{\sin(z)}{z^3}\right)^2 \end{aligned} \tag{5.33}$$

where

$$\lambda = a_\perp/R. \tag{5.34}$$

The more elongated the condensate is, the smaller λ will be.

And so $F_\epsilon(t)$ and $G(t)$ can be expressed as

$$F_\epsilon(t) = -2\dot{X}mN_1\Gamma \tag{5.35}$$
$$G(t) = 4k_BTmN_1\Gamma \tag{5.36}$$

where,

$$\Gamma = \frac{1}{2\pi}\frac{\hbar\mathcal{M}n_0^2\mathcal{I}}{R\sqrt{8\pi a_\perp^2}mN_1} \tag{5.37}$$

where,

$$\mathcal{I}(\lambda) = \int_0^\infty dz\ z^2\,\mathrm{erfcx}\left(\frac{\lambda z}{\sqrt{2}}\right)\left(\frac{4\sin(z)}{z^3} - \frac{4\cos(z)}{z^2}\right)^2 \tag{5.38}$$

Because the condensates are cigar shaped, they will be very elongated, so λ will be close to zero. As a reference we can find value of $\mathcal{I}$ at $\lambda = 0$ is

$$\mathcal{I}(0) = \frac{8}{3}\pi, \tag{5.39}$$

and $\mathcal{I}(\lambda)$ is plotted in Figure 5.1.

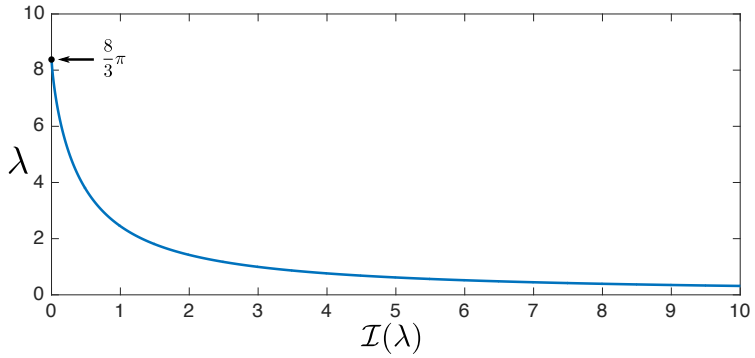

Figure 5.1: $\mathcal{I}$ plotted as a function of λ

Using Equations 5.7 and 5.10,

$$\Gamma = \frac{3}{16\pi}\frac{\hbar\mathcal{M}\Omega^2\mathcal{I}}{\sqrt{8\pi a_\perp^2 g}}. \tag{5.40}$$

Using the forms for $F(t)$ and $G(t)$ we now have the expression for the Langevin equation for the field momentum,

$$dP(t) = F(t)dt + \sqrt{G(t)}dW(t) \tag{5.41}$$
$$= \left(-\Omega^2 mN_1X - 2\dot{X}\Gamma mN_1\right)dt + \sqrt{4k_BTmN_1\Gamma}dW(t). \tag{5.42}$$
$$\tag{5.43}$$

We can thus find a Langevin equation for velocity of the centre of mass of the condensate

$$dV(t) = \frac{dP(t)}{mN_1} = -\Omega^2 X dt - 2\Gamma \dot{X} dt + \sqrt{\frac{4k_B T\Gamma}{mN_1}} dW(t), \tag{5.44}$$

defining the the centre of mass temperature,

$$\bar{T}_{CM} = \frac{k_B T}{mN_1}, \tag{5.45}$$

we derive,

$$dV(t) = -\Omega^2 X dt - 2\Gamma \dot{X} dt + \sqrt{4\bar{T}_{CM}\Gamma} dW(t). \tag{5.46}$$

This Langevin equation is the equation of motion of a classical simple harmonic oscillator, with damping coefficient Γ, and a random driving force. The main achievement here is that we have successfully gone from an equation with multiplicative noise, the energy-damped SPGPE (Equation 4.3), to an equation with only additive noise. Additive noise is much much easier to deal with numerically than multiplicative noise.

This derivation differs from the previous work [5], by numerical factors, and so it was essential to find these corrected results to allow us to compare the analytic expressions with numerical simulations of the full SPGPE.

5.1.3 Investigating Terms

In the form of the equation of motion for the centre of mass, Equation 5.46, we have defined two terms Γ and $\bar{T}_{CM}$, in Equations 5.40 and 5.45 respectively.

Γ has the role of the damping coefficient for the simple harmonic oscillator. It is linearly proportional to $\mathcal{M}$, so as the energy damping rate increases, the harmonic motion of the centre of mass is more strongly damped. This is also inversely proportional to the interaction strength of the particles in the condensate, so the damping is weaker for a more strongly damped condensate.

5.2 Two-time Correlation Functions

Correlation functions are a measure of correlated two variables are in space or time, there will be peaks for high levels of correlation, and the functions go to zero as the two variables become uncorrelated. This work relies on the use of the two-time correlation function, which gives a measure of how correlated a variable at one time t, is with the same variable at a different time t'. These may be expressed in the form

$$g_A(t, t') = \overline{A^*(t)A(t')} \tag{5.47}$$

where $g_A(t, t')$ is the two-time correlation function for the variable A at the times t and t'. The $\overline{\cdots}$ denotes an ensemble average over many independent trajectories.If the correlations of a variable with random fluctuations are only related to the time difference between the

samples, and not the absolute time, then the process is said to be *wide-sense stationary*. If this is the case, the two-time correlation function can be written as a function of only one variable, $\tau = t - t'$,

$$g_A(\tau) = \overline{A^*(t+\tau)A(t)}. \tag{5.48}$$

Two-time correlation functions can be used to characterise parameters such as the damping coefficient in systems influenced by random noise. $\bar{T}_{CM}$ influences the magnitude of the random noise acting on the simple harmonic oscillator. This increases with temperature, because we are measuring the effects of thermal noise. It also decreases with a larger total mass of the condensate, which is consistent with classical mechanics; the larger a mass is, the smaller the change in momentum due to an external force.

5.3 Damped Harmonic Oscillator with Random Driving Force

Because the centre of mass motion of the condensate can be described as a harmonic oscillator, we will first apply a classical treatment to investigate its analytical properties.

Equation 5.46 can be written in the form

$$dV(t) = -\Omega^2 X dt - 2\Gamma \dot{X} dt + \sqrt{4\bar{T}_{CM}\Gamma}\, dW(t) \tag{5.49}$$

$$\frac{dV}{dt} = -\Omega^2 X - 2\Gamma \dot{X} + \sqrt{4\bar{T}_{CM}\Gamma}\frac{dW(t)}{dt}. \tag{5.50}$$

Defining the noise term, $\xi(t) = \sqrt{4\bar{T}_{CM}\Gamma}\frac{dW(t)}{dt}$,

$$\ddot{X} + 2\Gamma\dot{X} + \Omega^2 X = \xi(t). \tag{5.51}$$

5.3.1 Two-Time Correlation Function of Position

We have a function of a variable X, with damping constant Γ, and an undamped frequency of Ω,

$$\ddot{X} + 2\Gamma\dot{X} + \Omega^2 X = \xi(t). \tag{5.52}$$

ξ can be expressed as an inverse Fourier transform

$$\xi(t) = \frac{1}{\sqrt{2\pi}}\int_{-\infty}^{\infty} d\omega e^{i\omega t}\Phi(\omega) \tag{5.53}$$

and conversely

$$\Phi(\omega) = \frac{1}{\sqrt{2\pi}}\int_{-\infty}^{\infty} dt e^{-i\omega t}\xi(t). \tag{5.54}$$

We assume that the two-time correlation function of $\xi(t)$ is time translation invariant

$$g_\xi(t,t') = \overline{\xi^*(t)\xi(t')} = f(t-t'). \tag{5.55}$$

The two-time correlation function of $\Phi(t)$ can be written using the Fourier transform of $\xi(t)$

$$\overline{\Phi^*(\omega)\Phi(\omega')} = \frac{1}{2\pi}\int_{-\infty}^{\infty} dt \int_{-\infty}^{\infty} dt' e^{i\omega t} e^{-i\omega' t'} \overline{\xi^*(t)\xi(t')} \tag{5.56}$$

$$= \frac{1}{2\pi}\int_{-\infty}^{\infty} dt \int_{-\infty}^{\infty} dt' e^{i\omega t - i\omega' t'} f(t-t'). \tag{5.57}$$

We do a wide-sense stationary variable transformation with $T = \frac{t+t'}{2}$, and $\tau = t - t'$, and find

$$\overline{\Phi^*(\omega)\Phi(\omega')} = \frac{1}{2\pi}\int_{-\infty}^{\infty} dT \int_{-\infty}^{\infty} d\tau e^{i\omega(T+\tau/2) - i\omega'(T-\tau/2)} f(\tau) \tag{5.58}$$

$$= \frac{1}{2\pi}\int_{-\infty}^{\infty} dT \int_{-\infty}^{\infty} d\tau e^{iT(\omega-\omega')} e^{i\tau\frac{\omega+\omega'}{2}} f(\tau) \tag{5.59}$$

$$= \delta(\omega-\omega')\sqrt{2\pi}F(\frac{\omega+\omega'}{2}), \text{ or} \tag{5.60}$$

$$\overline{\Phi^*(\omega)\Phi(\omega')} = \delta(\omega-\omega')\sqrt{2\pi}F(\omega), \tag{5.61}$$

where $F(\omega)$ is the inverse Fourier transform of $f(t)$.

Defining the Fourier transform of $X(t)$ as $\chi(\omega)$:

$$X(t) = \frac{1}{\sqrt{2\pi}}\int_{-\infty}^{\infty} d\omega e^{i\omega t}\chi(\omega) \tag{5.62}$$

and conversely

$$\chi(\omega) = \frac{1}{\sqrt{2\pi}}\int_{-\infty}^{\infty} dt e^{-i\omega t} X(t). \tag{5.63}$$

We can substitute Equations 5.53 and 5.62 into Equation 5.52

$$\frac{d^2}{dt^2}\int_{-\infty}^{\infty} d\omega e^{i\omega t}\chi(\omega) + 2\Gamma\frac{d}{dt}\int_{-\infty}^{\infty} d\omega e^{i\omega t}\chi(\omega) + \Omega^2\int_{-\infty}^{\infty} d\omega e^{i\omega t}\chi(\omega) = \int_{-\infty}^{\infty} d\omega e^{i\omega t}\Phi(\omega) \tag{5.64}$$

$$\int_{-\infty}^{\infty} d\omega e^{i\omega t}(\Omega^2 - \omega^2 + 2i\Gamma\omega)\chi(\omega) = \int_{-\infty}^{\infty} d\omega e^{i\omega t}\Phi(\omega). \tag{5.65}$$

And so:

$$(\Omega^2 - \omega^2 + 2i\Gamma\omega)\chi(\omega) = \Phi(\omega). \tag{5.66}$$

Thus,

$$\chi(\omega) = \frac{\Phi(\omega)}{\Omega^2 - \omega^2 + 2i\Gamma\omega}. \tag{5.67}$$

So we can express the two-time correlation function of $\chi(\omega)$ using Equation 5.61:

$$\overline{\chi^*(\omega)\chi(\omega')} = \frac{\sqrt{2\pi}F(\omega)\delta(\omega-\omega')}{(\Omega^2-\omega^2)^2+4\omega^2\Gamma^2}. \tag{5.68}$$

$X(t)$ is a stationary wide sense variable so $g_X(\tau) = \overline{X^*(t+\tau)X(t)}$ depends only on τ. Taking the Fourier transform and using Equations 5.62 and 5.68 we find:

$$\frac{1}{\sqrt{2\pi}}\int_{-\infty}^{\infty} d\tau \overline{X^*(t+\tau)X(t)}e^{-i\kappa\tau} = \frac{F(\kappa)}{(\Omega^2-\kappa^2)^2+4\kappa^2\Gamma^2}. \tag{5.69}$$

This is the power spectral density of $X(t)$.

$$\mathcal{F}\left[\overline{X^*(t+\tau)X(t)}\right](\kappa) = \frac{F(\kappa)}{(\Omega^2-\kappa^2)^2+4\kappa^2\Gamma^2}. \tag{5.70}$$

So we can take the inverse Fourier transform,

$$g_X(\tau) = \overline{X^*(t+\tau)X(t)} = \mathcal{F}^{-1}\left[\frac{F(\kappa)}{(\Omega^2-\kappa^2)^2+4\kappa^2\Gamma^2}\right](\tau), \tag{5.71}$$

which we can evaluate using the convolution theorem:

$$\mathcal{F}^{-1}(F\cdot G) = f * g. \tag{5.72}$$

Where

$$G(\kappa) = \frac{1}{(\Omega^2-\kappa^2)^2+4\kappa^2\Gamma^2}, \tag{5.73}$$

Taking the result from [19],

$$g(\tau) = \frac{1}{\sqrt{2\pi}}\int_{-\infty}^{\infty} d\kappa e^{i\kappa\tau}\frac{1}{(\Omega^2-\kappa^2)^2+4\kappa^2\Gamma^2} \tag{5.74}$$

$$= \frac{1}{\sqrt{2\pi}}\frac{\pi}{2\Gamma\Omega'\Omega}e^{-\Gamma|\tau|}\sin\left(\Omega'|\tau| + \sin^{-1}\left(\frac{\Omega'}{\Omega}\right)\right). \tag{5.75}$$

Where $\Omega' = \sqrt{\Omega^2-\Gamma^2}$, we are assuming $\Omega > \Gamma$.

Because $\xi(t)$ is delta-correlated, $\overline{\xi^*(t)\xi(t+\tau)} = f(\tau) = 4\bar{T}_{CM}\Gamma\delta(\tau)$.So,

$$g_X(\tau) = \mathcal{F}^{-1}(F\cdot G) \tag{5.76}$$

$$= f(\tau) * g(\tau) \tag{5.77}$$

$$= 4\bar{T}_{CM}\Gamma\delta(\tau) * \left[\frac{1}{\sqrt{2\pi}}\frac{\pi}{2\Gamma\Omega'\Omega}e^{-\Gamma|\tau|}\sin\left(\Omega'|\tau| + \sin^{-1}\left(\frac{\Omega'}{\Omega}\right)\right)\right] \tag{5.78}$$

$$\tag{5.79}$$

Giving us the analytical form of the two-time correlation function of position

$$g_X(\tau) = \frac{\bar{T}_{CM}}{\Omega'\Omega}e^{-\Gamma|\tau|}\sin\left(\Omega'|\tau| + \sin^{-1}\left(\frac{\Omega'}{\Omega}\right)\right). \tag{5.80}$$

5.3.2 Two-Time Correlation Function of Velocity

We can rewrite Equation 5.52 in terms of the velocity $V(t)$

$$\dot{V}(t) + 2\Gamma V(t) + \Omega^2 \int_{-\infty}^{t} V(t')dt' = \xi(t). \tag{5.81}$$

We define the Fourier transform of $V(t)$ as $\theta(\omega)$:

$$\theta(\omega) = \frac{1}{\sqrt{2\pi}} \int_{-\infty}^{\infty} dt e^{-i\omega t} V(t) \tag{5.82}$$

and conversely

$$V(t) = \frac{1}{\sqrt{2\pi}} \int_{-\infty}^{\infty} d\omega e^{i\omega t} \theta(\omega). \tag{5.83}$$

Using Equation 5.83 to rewrite Equation 5.81,

$$\frac{d^2}{dt^2} \int_{-\infty}^{\infty} d\omega e^{i\omega t}\theta(\omega) + 2\Gamma \int_{-\infty}^{\infty} d\omega e^{i\omega t}\theta(\omega) + \Omega^2 \int_{-\infty}^{t} dt' \int_{-\infty}^{\infty} d\omega e^{i\omega t'}\theta(\omega) = \int_{-\infty}^{\infty} d\omega e^{i\omega t}\Phi(\omega)$$

$$\int_{\infty}^{\infty} d\omega e^{i\omega t} \left(i\omega\theta(\omega) + 2\Gamma\theta(\omega) + \frac{\Omega^2}{i\omega}\theta(\omega) \right) = \int_{-\infty}^{\infty} d\omega e^{i\omega t}\Phi(\omega).$$

So,

$$\Phi(\omega) = \left(i\omega + 2\Gamma + \frac{\Omega^2}{i\omega} \right) \theta(\omega), \tag{5.84}$$

and similarly, to before,

$$\theta(\omega) = \frac{\Phi(\omega)}{\left(i\omega + 2\Gamma + \frac{\Omega^2}{i\omega} \right)}. \tag{5.85}$$

We can express this in terms of $\chi(\omega)$ using Equation 5.67

$$\theta(\omega) = i\omega\chi(\omega), \tag{5.86}$$

and so we can calculate the two-time correlation function of $\theta(\omega)$

$$\overline{\theta^*(\omega)\theta(\omega')} = \frac{\omega^2\sqrt{2\pi}F(\omega)\delta(\omega - \omega')}{(\Omega^2 - \omega^2)^2 + 4\omega^2\Gamma^2}. \tag{5.87}$$

Using the result from Equation 5.70,

$$\mathcal{F}\left[\overline{V^*(t+\tau)V(t)}\right](\kappa) = \frac{\kappa^2 F(\kappa)}{(\Omega^2 - \kappa^2)^2 + 4\kappa^2\Gamma^2}. \tag{5.88}$$

So we can take the inverse Fourier transform,

$$g_V(\tau) = \overline{V^*(t+\tau)V(t)} = \mathcal{F}^{-1}\left[\frac{\kappa^2 F(\kappa)}{(\Omega^2 - \kappa^2)^2 + 4\kappa^2\Gamma^2} \right](\tau), \tag{5.89}$$

again we use the convolution theorem

$$g_V(\tau) = \overline{V^*(t+\tau)V(t)} = \mathcal{F}^{-1}\left[H \cdot G\right] = h * g. \tag{5.90}$$

Here $G(\kappa)$ and $g(t)$ are the same as Equations 5.73 and 5.75 respectively, and $H = \kappa^2 F(\kappa)$. So $h(t) = -\frac{d^2}{dt^2} f(t)$, and again if $\xi(t)$ is delta correlated, $h(t) = -4\bar{T}_{CM}\Gamma\delta''(t)$. So,

$$g_V(\tau) = -4\bar{T}_{CM}\Gamma\delta''(t) * \left[\frac{1}{\sqrt{2\pi}}\frac{\pi}{2\Gamma\Omega'\Omega}e^{-\Gamma|\tau|}\sin\left(\Omega'|\tau| + \sin^{-1}\left(\frac{\Omega'}{\Omega}\right)\right)\right] \tag{5.91}$$

$$= -\frac{d^2}{d\tau^2}\frac{\bar{T}_{CM}}{\Omega'\Omega}e^{-\Gamma|\tau|}\sin\left(\Omega'|\tau| + \sin^{-1}\left(\frac{\Omega'}{\Omega}\right)\right). \tag{5.92}$$

Assuming that $\Omega > \Gamma$,this equals

$$g_V(\tau) = -\frac{\bar{T}_{CM}}{\Omega\Omega'}e^{-\Gamma|\tau|}\left[\left(2\Gamma^2 - \Omega^2\right)\sin\left(\Omega'|\tau| + \sin^{-1}\left(\frac{\Omega'}{\Omega}\right)\right)\right.$$
$$\left. -2\Omega'\Gamma\cos\left(\Omega'|\tau| + \sin^{-1}\left(\frac{\Omega'}{\Omega}\right)\right)\right]. \tag{5.93}$$

The two-time correlation function of velocity is equal to the negative second time derivative of the two-time correlation function of position,

$$g_V(\tau) = -\frac{d^2}{d\tau^2}g_X(\tau). \tag{5.94}$$

For $\Omega = 1$, both $g_X(\tau)$ and $g_V(\tau)$ have the same decay envelope, defined by

$$g_{decay}(\tau) = \bar{T}_{CM}\,\mathrm{e}^{-\Gamma|\tau|}. \tag{5.95}$$

5.4 Equipartition Theorem

The value of a two-time correlation function of a variable at $\tau = 0$ is the same as the ensemble average for the variable squared:

$$g_A(\tau = 0) = \overline{A^*(t+\tau)A(t)}|_{\tau=0} = \overline{|A(t)|^2}. \tag{5.96}$$

We have analytical forms for the two-time correlation functions on position and velocity (Equations 5.80 and 5.93), which allow us to find the average potential and kinetic energy of the harmonic oscillator system, which should be the same as the potential and kinetic energy of the centre of mass of the condensate.

Substituting in $\tau = 0$, we find

$$g_X(0) = \overline{X^*(t+0)X(t)} = \overline{X(t)^2} = \frac{\bar{T}_{CM}}{\Omega^2} \tag{5.97}$$

$$g_V(0) = \overline{V^*(t+0)V(t)} = \overline{V(t)^2} = \bar{T}_{CM}. \tag{5.98}$$

And so the average potential energy, E_p, and kinetic energy, E_k for a condensate of mass $M = N_1 m$ are

$$E_p = \frac{1}{2} M \Omega^2 \overline{X^2} = \frac{1}{2} M \Omega^2 \frac{\bar{T}_{CM}}{\Omega^2} = \frac{1}{2} M \bar{T}_{CM}, \tag{5.99}$$

and,

$$E_k = \frac{1}{2} M \overline{V^2} = \frac{1}{2} M \bar{T}_{CM}. \tag{5.100}$$

Using the definition of the centre of mass temperature (Equation 5.45), $\bar{T}_{CM} = \frac{k_B T}{m N_1}$,

$$E_p = E_k = \frac{1}{2} k_B T. \tag{5.101}$$

Thus each degree of freedom of the centre of mass of the condensate (kinetic and potential) contribute $\frac{1}{2} k_B T$ to the total energy, satisfying the equipartition theorem.

The average total energy of the centre of mass of the condensate is

$$E_{total} = k_B T. \tag{5.102}$$

5.5 Simple Harmonic Oscillator Simulations

To test our analytic results a simulations of a damped simple harmonic oscillator with a random driving force were performed.

5.5.1 Numerical Simple Harmonic Oscillator Simulation Method

The simple harmonic oscillator with random driving force was simulated using an Euler method.

This calculates the value of position and velocity at discrete time intervals Dt by further dividing this into smaller time intervals dt.

A vector $\mathbf{Y}$ of position and velocity is defined,

$$\mathbf{Y} = \begin{bmatrix} \mathbf{X} \\ \mathbf{V} \end{bmatrix} \tag{5.103}$$

$\mathbf{Y}$ is calculated at time $t + dt$, from the value of $\mathbf{Y}$ at time t,

$$\mathbf{Y}(t + dt) = \mathbf{Y}(t) + \mathbf{h}(t, \mathbf{Y}(t)) dt \tag{5.104}$$

where,

$$\mathbf{h}(t, \mathbf{Y}(t)) = \begin{bmatrix} \mathbf{Y}_2(t) \\ \Xi(t) - 2\Gamma \mathbf{Y}_2(t) - \Omega^2 \mathbf{Y}_1(t) \end{bmatrix} \tag{5.105}$$

and the random increment $\Xi(t)$ is defined as

$$\Xi(t) = \sqrt{\frac{4 \bar{T}_{CM} \Gamma}{dt}} \bar{\xi}(t) \tag{5.106}$$

$\bar{\xi}(t)$ is a delta correlated random variable with a Gaussian probability distribution centred at 0 with a variance of 1.

5.5.2 Two-Time Correlation Function Calculations

The SPGPE simulations or harmonic oscillator simulations are used to generate values for the position and velocity at different times. These simulations are performed multiple times to give a large ensemble. The values are stored in matrices, where each column is for one ensemble and each row is at a specific time,

$$\begin{bmatrix} X(t_1)_1 & X(t_1)_2 & \dots \\ X(t_2)_1 & X(t_2)_2 & \dots \\ \vdots & \vdots & \end{bmatrix} \tag{5.107}$$

Each column, $\mathbf{X}(t)_i$, is multiplied by its Hermitian conjugate to give a square matrix $\mathbf{X}(t)_i\mathbf{X}^*(t')_i$, and then an ensemble average is performed

$$\overline{\mathbf{X}(t)\mathbf{X}^*(t')} = \frac{1}{N}\sum_i^N \mathbf{X}(t)_i\mathbf{X}^*(t')_i. \tag{5.108}$$

This results in the two-time correlation function evaluated at discrete values of t and t'. This is symmetrical around $t = t'$, and so we can find the two-time correlation function as just a function of τ, $\overline{X^*(t+\tau)X(t)}$. This is done by performing a skew so that the $t = t'$ line is at $\tau = 0$, and then performing an average along the vertical direction (Figure 5.2). This means that more elements are averaged over for τ closer to 0, and the number of elements decreases for a larger magnitude of τ.

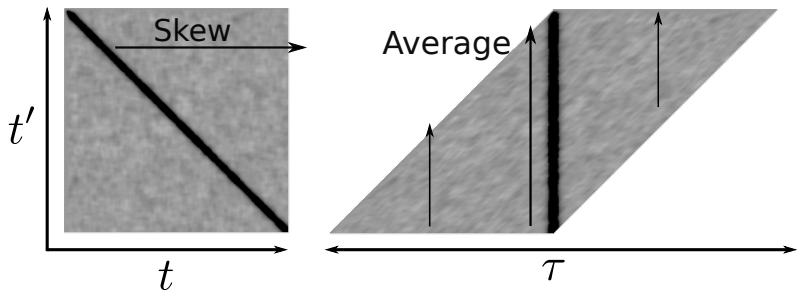

Figure 5.2: Visual representation of how the two-time correlation function is averaged. The two-time correlation function, as a function of t and t' is skewed, and then an average is performed over the non-zero element in each column. This gives the two-time correlation function as a function of τ.

5.6 Numerical SHO Results

To test the validity of the analytic forms for the two-time correlation functions of position and velocity, these were compared with two-time correlation functions found using the simple harmonic oscillator simulations detailed in Sections 5.5.1 and 5.5.2. These simulations provide a simple way to test the analytic results, and are independent of the SPGPE.

Using simulation parameters of the undamped frequency Ω, damping coefficient Γ and the centre of mass temperature $\bar{T}_{CM}$, simulations for the simple harmonic oscillator with a random driving force (Equation 5.52) were performed. These simulations were carried out for the underdamped case, $\Gamma < \Omega$ as this was the case for which the analytic forms were found. The position and velocity were calculated as a function of t, for many trajectories, one realisation of which is shown in Figure 5.3

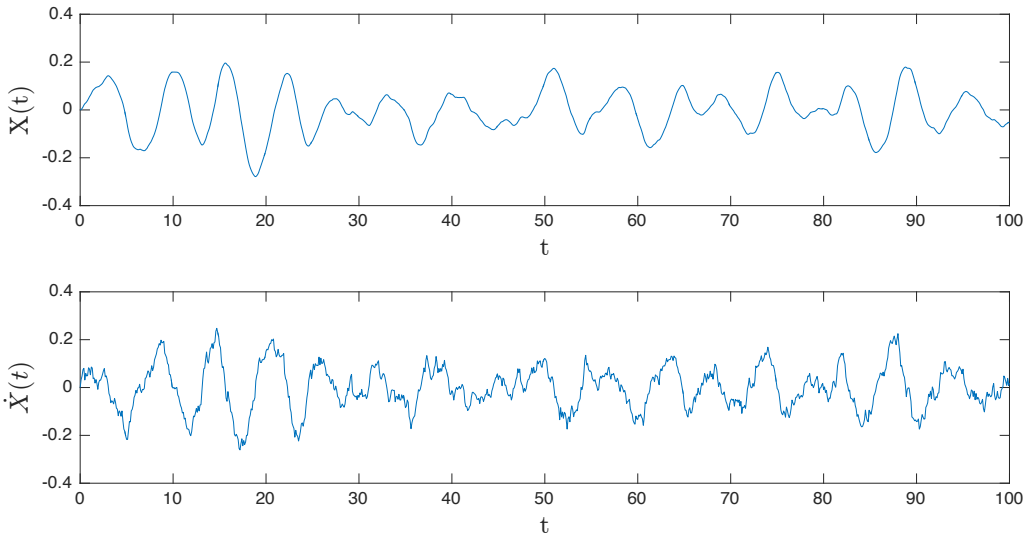

Figure 5.3: The position and velocity of a simple harmonic oscillator subject to a random driving force, with $\Omega = 1$, $\Gamma = 0.1$ and $\bar{T}_{CM} = 0.01$. In the undriven case, the choice of units for position and time may be scaled, but in the driven case, the units are set with respect to the driving force.

Two-time correlation functions were computed for these simulations, showing close to analytic agreement for large enough ensembles (Figure 5.4).

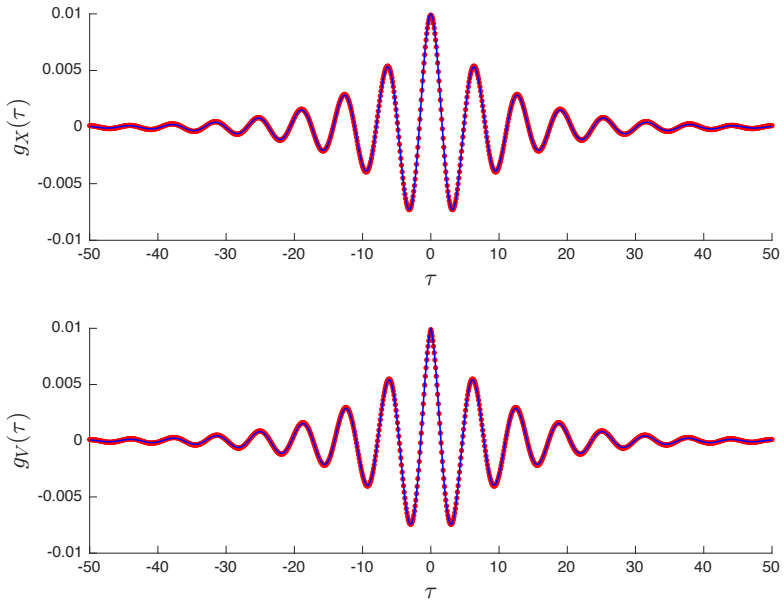

Figure 5.4: The analytic (blue lines) and simulated (red points) two-time correlation functions for position and velocity for the simple harmonic oscillator with a random driving force. The parameters are $\Omega = 1$, $\Gamma = 0.1$ and $\bar{T}_{CM} = 0.01$, and an ensemble of 1000 trajectories was averaged over.

Chapter 6

SPGPE Simulations

In this section we discuss the condensate simulations of the full SPGPE, the choice of dimensionless units and parameters. The analytic and simulation results are compared using two-time correlation functions for the condensate centre of mass.

6.1 Numerical Preliminaries for Condensate Simulations

6.1.1 Dimensionless Units

In computational physics it is common to define a set of dimensionless units for numerical ease and notational simplicity. When dealing with a harmonically trapped system all the natural units are defined with respect to the trapping frequency. There are several distinct trapping frequencies in this regime, but because we are concerned with the behaviour of the condensate in the longitudinal direction we choose $\Omega = \omega_{x,1}$ from which to define our units. Our unit of time is simply the inverse of the trap frequency,

$$t_0 = 1/\Omega, \tag{6.1}$$

the length unit is the harmonic oscillator length of the trap

$$l_0 = a_{x,1} = \sqrt{\frac{\hbar}{m_1\Omega}}. \tag{6.2}$$

By defining these units, the other units for the simulations are also set, the mass unit is simply the mass of a single component 1 particle,

$$m_0 = m_1, \tag{6.3}$$

the energy unit is the characteristic energy of the trap

$$E_0 = \hbar\Omega, \tag{6.4}$$

which allows us to define the temperature unit,

$$T_0 = \frac{\hbar\Omega}{k_B}. \tag{6.5}$$

These units are then used to define our simulation constants in dimensionless forms, which are denoted by a tilde. The energy damping rate, $\mathcal{M}$, becomes

$$\tilde{\mathcal{M}} = \frac{8\pi\tilde{a}_{12}}{\mathrm{e}^{-\tilde{\mu_2}/\tilde{T}} - 1}, \tag{6.6}$$

where $\tilde{a}_{12}$ is the dimensionless cross scattering length between the cloud and the condensate, $\tilde{a}_{12} = a_{1,2}/a_{x,1}$; $\tilde{\mu}_2$ is the dimensionless form of the chemical potential of component 2, $\tilde{\mu}_2 = \mu_2/\hbar\Omega$; and $\tilde{T}$ is the Temperature in dimensionless units, $\tilde{T} = T\ k_B/\hbar\Omega$.

The nonlinear interaction coefficient has the dimensionless form

$$\tilde{g} = 2\tilde{a}_{11}\tilde{\omega}_{\perp,1}, \tag{6.7}$$

where $\tilde{a}_{11}$ is the dimensionless scattering length between particles in component 1, and $\tilde{\omega}_{\perp,1}$ is the ratio of the transverse trapping frequency of the condensate to the chosen reference frequency Ω.

Hence we expect that the damping coefficient of the simulations will be given by,

$$\tilde{\Gamma} = \frac{3}{16\pi}\frac{\tilde{\mathcal{M}}\mathcal{I}(\lambda)}{\sqrt{8\pi\tilde{a}_{\perp,1}^2}\tilde{g}}. \tag{6.8}$$

$\mathcal{I}(\lambda)$ (Equation 5.38) is unaffected by the choice of units, because it is dimensionless and is a function of λ, which is also dimensionless (Equation 5.34).

6.1.2 Simulation Parameters

For choosing our simulation parameters we need to be able to ensure that our system requirements are satisfied,

$$T_{c,2} \lesssim T < T_{c,1} \tag{6.9}$$

and

$$\frac{\hbar^2}{ma_{11}^2} \ll \mu_1 < \hbar\omega_{\perp,1}. \tag{6.10}$$

And also that the system parameters are experimentally realisable. For the thermal cloud, the trap frequencies do not need to be especially tight, and so the main restriction is on how shallow they can be. Experimentally, ultracold atoms have successfully been confined in traps with frequencies as low as 6.1 Hz [20]. For component 1, the transverse trapping frequency must be very high to ensure it is pseudo 1D, experimentally traps as tight as $2\pi\times$ 790 Hz [21] and $2\pi \times 850$ Hz [22, 23]. For the temperature regime, the first experimentally achieved BEC in an atomic vapour was made at 170 nK, and was subsequently cooled to

20 nK [1]. For BEC confined to one dimension the particle number is often in the order of 10^4 [21].

For running numerical simulations many, trajectories are performed with identical initial conditions, but a different realisation of the noise. The initial wavefunction for the SPGPE simulations is a Thomas-Fermi wavefunction of the form

$$\tilde{\psi}_{init}(x) = \tilde{\psi}_{TF}(x) = \mathrm{Re}\left[\sqrt{\frac{1}{\tilde{g}}\left(\tilde{\mu}_1 - \frac{1}{2}\tilde{x}^2\right)}\right]. \tag{6.11}$$

This has to be allowed to thermalise, and so the simulations must be run for at least 2 to 3 damping times to allow for the transient initial behaviour to die out, where the damping time is defined by $1/\tilde{\Gamma}$. This means that to run the simulations, $\tilde{\Gamma}$ has to be large enough so that the simulations can be run in a reasonable amount of time.$\tilde{\Gamma}$ can be tuned by changing the parameters to allow the simulations to be performed in a reasonable time. There are strict restrictions on the geometry of component 1, so ideally these parameters wouldn't be used to tune $\tilde{\Gamma}$. $\tilde{g}$ is determined by the choice of atoms in component 1, and the geometry of component 1, and so also isn't useful for tuning $\tilde{\Gamma}$. This leaves $\tilde{\mathcal{M}}$ for tuning $\tilde{\Gamma}$, which is ideal because it can be varied by changing the geometry of component 2 which has a lot of freedom. $\tilde{\mathcal{M}}$ depends directly on the chemical potential of component 2, which in turn depends on the geometry and number of particles of component 2. Because component 2 is a thermal cloud it is well approximated as an ideal gas with no interactions, and $\tilde{\mu}_2$ can be found by numerically solving

$$N_2 = \frac{(\tilde{T}\ \Omega)^3}{\omega_{x,2}\ \omega_{\perp,2}^2}\ g_3\left(\exp\left(\frac{\tilde{\mu}_2}{\tilde{T}}\right)\right), \tag{6.12}$$

where $g_n(z)$ is the normal definition of the Bose function, $g_n(z) = \sum_{j=1}^{\infty}(z^j/j^n)$ [17].

Because $g_n(z)$ is increasing over the range in which it is defined, by increasing $\omega_{\perp,2}$ while holding N_2 constant, $\tilde{\mu}_2$ may be increased up to a maximum value of $\tilde{\mu}_2 = 0$, which corresponds to component 2 being at its critical temperature,

$$\tilde{T}_{c,2} = \tilde{\bar{\omega}}_2\left(\frac{N_2}{\zeta(3)}\right)^3, \tag{6.13}$$

where $\tilde{\bar{\omega}}_2$ is the dimensionless geometric mean trap frequency for component 2.

By increasing $\omega_{\perp,2}$ to increase $\tilde{\mu}_2$ to close to zero, this will make the denominator of Equation 6.6 much smaller, thus increasing $\tilde{\mathcal{M}}$.In these simulations $\tilde{\Gamma}$ was tuned to around 0.1, which allows for the system to quickly thermalise while still being underdamped, which in this case means $\tilde{\Gamma} < 1$.

Component 1 is assumed to remain Thomas-Fermi, and thus the dimensionless chemical potential is given by

$$\tilde{\mu}_1 = \frac{1}{2}\left(\frac{3}{2}N_1\tilde{g}_1\right)^{2/3}. \tag{6.14}$$

For the simulations, the trap geometries are set, as well as the system temperature and the number of particles in each component. The atomic species in each trap must also be chosen, which will set the scattering lengths and masses. By setting these parameters, other variables such as the chemical potential of each component is also set.

6.1.3 Numerical Evaluation of Position and Momentum Centre of Mass

Because the condensate wavefunction was evaluated in the harmonic oscillator basis, it is easiest to evaluate the position and momentum expectation values in this basis also.

The numeric position and momentum operators can be constructed from the standard harmonic oscillator creation and annihilation operators,

$$\hat{x} = \frac{1}{\sqrt{2}}(\hat{a} + \hat{a}^\dagger) \tag{6.15}$$

$$\hat{p} = -i\frac{1}{\sqrt{2}}(\hat{a} - \hat{a}^\dagger), \tag{6.16}$$

where $\hat{a}$ and $\hat{a}^\dagger$ are square matrices of dimension E_{cut},

$$\hat{a} = \begin{pmatrix} 0 & \sqrt{1} & 0 & \dots \\ 0 & 0 & \sqrt{2} & \dots \\ 0 & 0 & 0 & \ddots \\ \vdots & \vdots & \vdots & \ddots \end{pmatrix}, \qquad \hat{a}^\dagger = \begin{pmatrix} 0 & 0 & 0 & \dots \\ \sqrt{1} & 0 & 0 & \dots \\ 0 & \sqrt{2} & 0 & \dots \\ \vdots & \vdots & \ddots & \ddots \end{pmatrix} \tag{6.17}$$

The wavefunction is calculated as a column vector, $\psi(x,t) = \boldsymbol{\psi}$, and so the position and momentum expectation values and normalisation can be found with simple discrete matrix multiplication,

$$\langle \hat{x} \rangle = \boldsymbol{\psi}^\dagger \cdot \hat{x} \cdot \boldsymbol{\psi} \tag{6.18}$$

$$\langle \hat{p} \rangle = \boldsymbol{\psi}^\dagger \cdot \hat{p} \cdot \boldsymbol{\psi} \tag{6.19}$$

$$N_1 = \boldsymbol{\psi}^\dagger \cdot \boldsymbol{\psi} \tag{6.20}$$

where $\boldsymbol{\psi}^*$ is the matrix Hermitian conjugate of $\boldsymbol{\psi}$.

6.2 SPGPE Simulations

The simulations were performed for two different systems; a condensate of ^{87}Rb with a thermal cloud of ^{87}Rb, and a condensate of ^{23}Na with a thermal cloud of ^{87}Rb. For the first case where both the thermal cloud and condensate are ^{87}Rb, this system can be treated as number conserving if the two components are in different spin states and we ignore the effect of spin changing interactions. For the case of the ^{23}Na condensate with the ^{87}Rb thermal cloud, there will be an additional factor in $\mathcal{M}$ that is currently unknown,

due to the mass difference between scattering particles. This unknown factor will not vary in position or space, and so because Γ is linearly proportional to $\mathcal{M}$ this will just mean that there is additional factor in the form of Γ. This factor is thought to be of order 2, and so will not change the results dramatically, although it is currently undetermined.For both cases $\omega_{\perp,2}$ was used to tune the analytic $\tilde{\Gamma}$ to be around 0.1. The simulations were performed over a range of temperatures using the constant geometry for component 1, and keeping $\omega_{x,2}$ held constant.

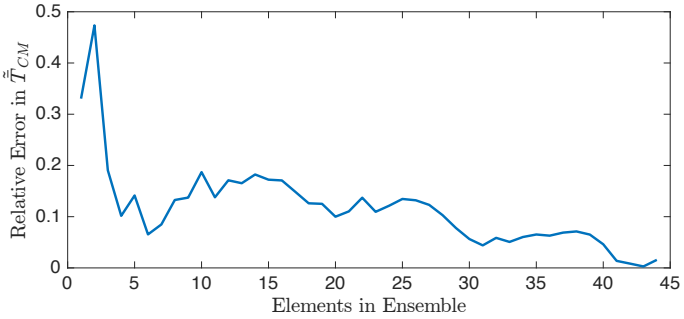

Figure 6.1: Relative error in $\bar{T}_{CM}$ with different ensemble sizes

6.2.1 Ensembles and Statistical Convergence

Using the SPGPE, the interaction effects between the condensate and the thermal cloud are treated stochastically. For this reason, steady state ensemble phenomena, such as the two-time correlation function, must be found by performing an ensemble average over many independent trajectories. Many trajectories are performed simultaneously using parallel computing; because each of these trajectories are independent, the task is embarrassingly parallel and is simple to implement.

Furthermore, because the centre of mass properties at one time become effectively un-

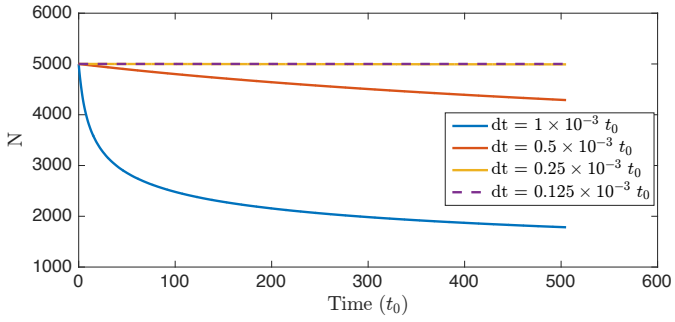

Figure 6.2: The number of particles in a simulated condensate, for different Euler timesteps. Because the number of particles is constant for our model, this method is unstable for timesteps greater than $dt = 0.25 \times 10^{-3}\ t_0$. The method is convergent for $dt = 0.25 \times 10^{-3}\ t_0$, because halving this timestep to $dt = 0.125 \times 10^{-3}\ t_0$ still gives the same behaviour.

correlated after around 3 damping times, one long trajectory may be split into smaller trajectories that can be treated as independent. This means that for each of the smaller trajectories the system is already in a thermalised state, and there is no need to wait for the transient Thomas-Fermi behaviour to decay. For a larger ensemble with more trajectories, the agreement between the analytic and simulated data becomes much better. This can be seen in Figure 6.1, where the relative error in $\bar{T}_{CM}$ approaches zero as more trajectories are averaged over.

Numerical Convergence

It is important to test there is numerical convergence when using numerical differential equation solvers, such as are used here for solving the SPGPE. If the Euler timestep is too low, then the results do not converge, as is shown in Figure 6.2. Convergence is seen when the simulations have the same behaviour when the timestep is halved.

The position and velocity, and hence the two-time correlation functions were found using methods described in Sections 6.1.3 and 5.5.2 (Figure 6.4). The simulated results were compared with the analytic forms of the position and momentum two-time correlation functions (Equations 5.80 and 5.93), using analytic forms for $\tilde{\Gamma}$ and $\tilde{\bar{T}}_{CM}$, Equations 5.40 and 5.45. Because we are working in units defined by the the longitudinal frequency for component 1, Ω in Equations 5.80 and 5.93 is set to unity.

Computation Requirements

To simulate the condensate using the SPGPE (Equation 4.3), a Semi-Implicit Euler method was used[24]. These simulations were performed in parallel on machines using 6 core Intel core-i7 3930K 3.2GHz processors and 64Gb of physical memory. The typical length of a simulation ranged from 8 hours to 2 days. The total elapsed time for all simulations for this project was around 70 days – i.e., running all of the simulations on a machine with a single core would take around 420 days.

6.2.2 ^{87}Rb Condensate Simulations

For the full SPGPE simulations using a condensate and cloud of ^{87}Rb, the trapping frequencies and component populations were set to ensure a pseudo 1D condensate that was numerically suitable. The constant trapping frequencies were $\Omega = 62.8$ Hz, $\omega_{\perp,1} = 5340$ Hz, $\omega_{x,2} = 56.5$ Hz. The component populations were $N_1 = 5710$ and $N_2 = 10^6$. The ^{87}Rb-^{87}Rb s-wave scattering length is $a_s = a_{11} = a_{12} = 98a_0$, and so the dimensionless non-linear interaction coefficient for these simulations is $\tilde{g} = 0.259$ and the dimensionless chemical potential of component 1, which is assumed to be Thomas-Fermi, is $\tilde{\mu}_1 = 84.4$. For the different temperature simulations $\omega_{\perp,2}$ was varied which effected the other simulation parameters, as shown in Table 6.1. These simulations were performed using a semi implicit Euler method, calculating the state of the wavefunction every 0.0785 t_0 from $t = 0$ t_0 to $t = 1000$ t_0. The analytic damping time for all the simulations was around $1/\tilde{\Gamma} = 10$, and so these were split into trajectories running for 50 t_0 each, discounting the

$\tilde{T}$	T (nk)	$\omega_{\perp,2}$ (Hz)	$\tilde{\mu}_2$	$\tilde{\mathcal{M}}$	$\tilde{\Gamma}$	$\tilde{\bar{T}}_{CM}$
20	9.60	6.4861	-0.0392	0.0296	0.102	0.004
30	14.4	11.9	-0.0554	0.0314	0.108	0.006
40	19.2	18.3	-0.0741	0.0314	0.108	0.008
50	24.0	25.6	-0.0894	0.0325	0.111	0.01
60	28.8	33.7	-0.101	0.0345	0.111	0.012
70	33.5	42.5	-0.128	0.0318	0.109	0.014
77.74	37.3	49.7	-0.137	0.0330	0.113	0.0155
90	43.2	61.9	-0.167	0.0314	0.108	0.018
150	72.0	133	-0.273	0.0319	0.109	0.03

Table 6.1: Consistent parameters for SPGPE simulations of a pseudo-1D condensate of ^{87}Rb in a 3D thermal cloud of ^{87}Rb. These parameters are chosen such that the system temperature is greater than the critical temperature for the thermal cloud, and lower than the critical temperature for the condensate.

first trajectory to allow for the system to thermalise. 6 simulations were run in parallel resulting in a total of 120 trajectories for each set of parameters.

For low temperatures, there is excellent agreement between the analytic and simulated two-time correlation functions, for both position and velocity. Especially for small $\tilde{\tau}$, the agreement is very good; the tails deviate more from the analytic result due to averaging over a smaller number of samples, as described in Section 5.5.2. For both the $\tilde{T} = 20$ and $\tilde{T} = 60$ results there is very little disagreement between the analytic and numerical results. For $\tilde{T} = 77.74$, which is the chemical potential of the condensate, the decay rate of the simulated results begins to differ more from the analytic results, and this trend is shown at higher temperature at $\tilde{T} = 150$, with even more deviation. Deviation at high temperature is expected because the analytic forms of the decay time are based on the assumption that the wavefunction had the form of the Thomas-Fermi state, with an offset from the centre of the trap. Because the Thomas-Fermi is a zero temperature solution to the GPE for a system with a given chemical potential, we would expect the analytic results to only be valid for temperatures which are small compared to the chemical potential, $\tilde{T} < \tilde{\mu}_1$. Comparing the error in $\tilde{\Gamma}$ against different temperature, we can see that the relative error between the damping coefficient from the simulations and analytic results becomes greater for $\tilde{T} > \tilde{\mu}_1$ (Figure 6.3). Here the error is relative error, defined as

$$\textit{Relative Error in } \tilde{\Gamma} = \frac{\tilde{\Gamma}_{fitted} - \tilde{\Gamma}_{analytic}}{\tilde{\Gamma}_{analytic}}, \tag{6.21}$$

where $\tilde{\Gamma}_{fitted}$ was found by numerically fitting an exponential decay curve to the peaks of $g_X(\tau)$ from the simulated data.

Although at higher temperatures the damping coefficient becomes less well described by the analytic form, the frequency term Ω appears to remain consistent. This is because although for higher temperatures the wavefunction is no longer well described by a Thomas Fermi

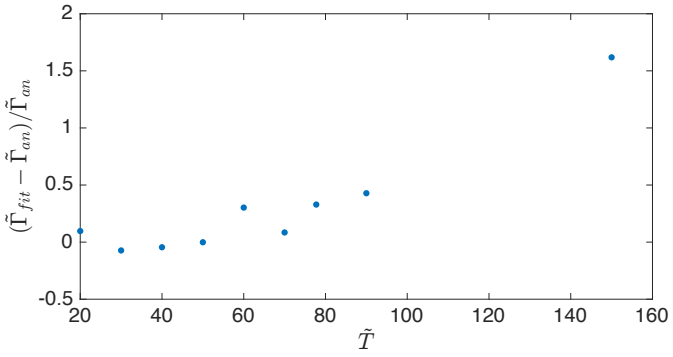

Figure 6.3: The relative error in the dimensionless damping coefficient for different system temperatures, for the ^{87}Rb simulations.

state, the oscillation $-\omega^2 X dt$ term in Equation 5.46, depends only on the centre of mass position of the wavefunction and not on actual form of the wavefunction.

Penrose-Onsager Criterion

To investigate the temperature regime more deeply, it is useful to see how closely the condensate resembles a Thomas-Fermi state. The condensate fraction and corresponding wavefunction can be found using the Penrose-Onsager criterion.

For finite temperature BEC, there will be a fraction that is in the ground state, which is referred to as the condensate fraction, and there will be other excited modes which are uncondensed. The occupation and spatial distribution of the 'orbitals' can be found using the Penrose-Onsager criterion. This is done by finding a 1-body density matrix for the state by performing an ensemble average over many outer products of independent states,

$$\hat{\rho}(x, x') = \langle \psi(x)\psi(x') \rangle \tag{6.22}$$

The eigenstates of $\hat{\rho}$ will give the spatial distributions of each of the orbitals, and the corresponding eigenvalues give the occupation:

$$\int dx' \ \hat{\rho}(x, x')\phi_n(x') = N_n \phi_n(x), \tag{6.23}$$

where $\phi_n(x)$ is the spatial distribution of the orbital with occupation N_n. The eigenstate corresponding to the largest eigenvalue will be the ground state of the BEC, and the eigenstate with the second largest eigenvalue will be the first excited state.

As the temperature increases it can be seen in Figure 6.4 that the condensate fraction wavefunction begins to lose Thomas-Fermi character and begins to approach a Gaussian form. As well as becoming less like the zero temperature Thomas Fermi solution, the population of the condensate fraction also decreases as temperature increases(Figure 6.5).

Although this decline in the condensate fraction is expected, it is very different from what is predicted by [17], this is because our thermodynamic regime is a canonical ensemble

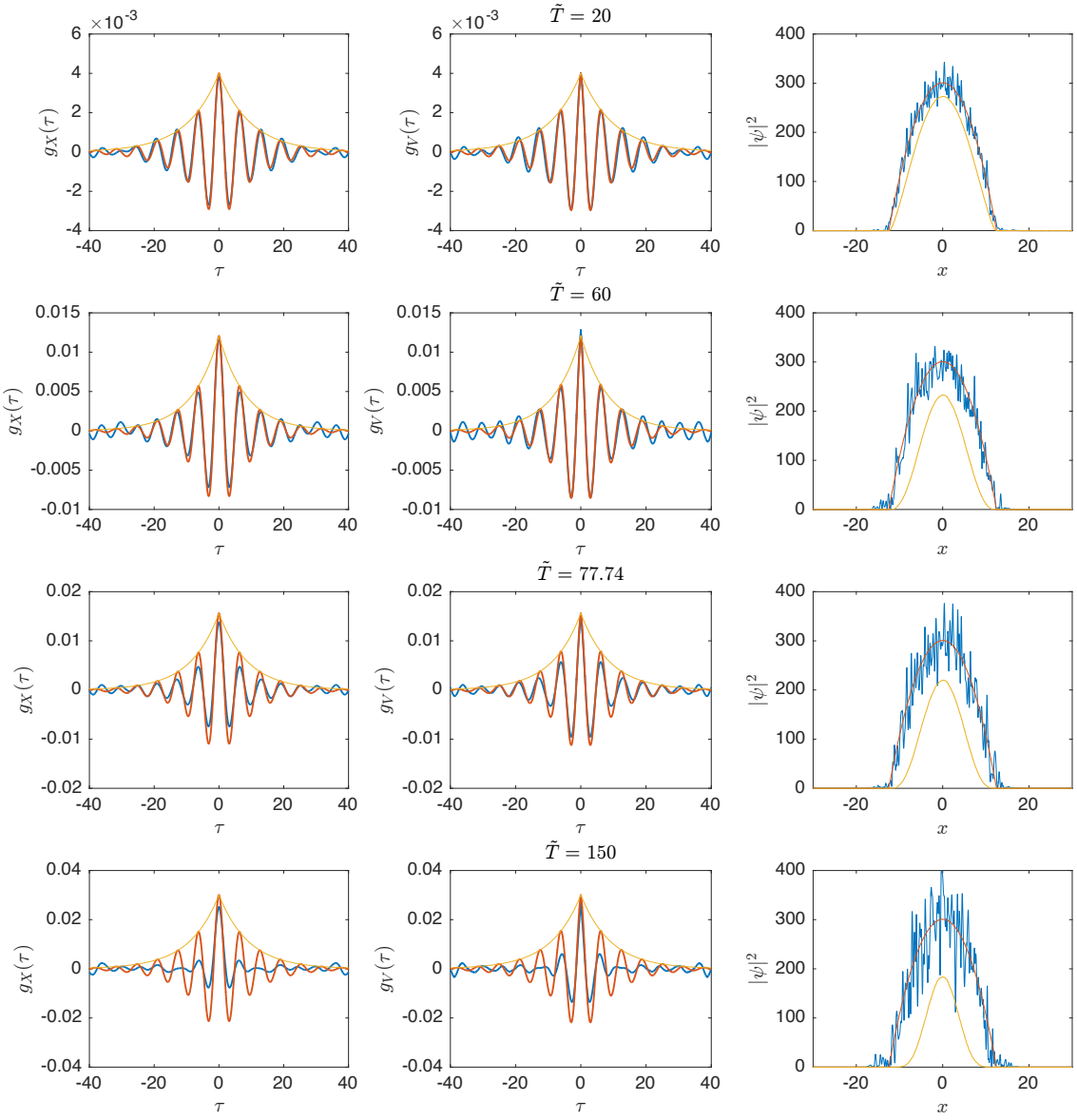

Figure 6.4: Plots of two-time correlation functions versus time, for a condensate of ^{87}Rb over a range of temperatures $\tilde{T} = 20, 60, 77.74, 90$; also shown are condensate densities (right column). The analytic forms for $g_X(\tau)$ (5.80) and $g_V(\tau)$ (5.93) are plotted in the first and second column (orange) together with the results from the SPGPE simulations (blue), and the analytic decay envelope, (5.95) (yellow). In the third column we plot the particle densities for the zero-temperature Thomas-Fermi solution (2.9) (red), the condensate orbital obtained using the Penrose-Onsager criterion (6.22, 6.23), and a particular SPGPE trajectory (blue). τ is in units of $1/\Omega$, x is in units of $a_{x,1}$.

rather than a grand canonical ensemble, and also because for a tightly confined 1D condensate the interactions between particles will cause deviations away from the ideal gas prediction.

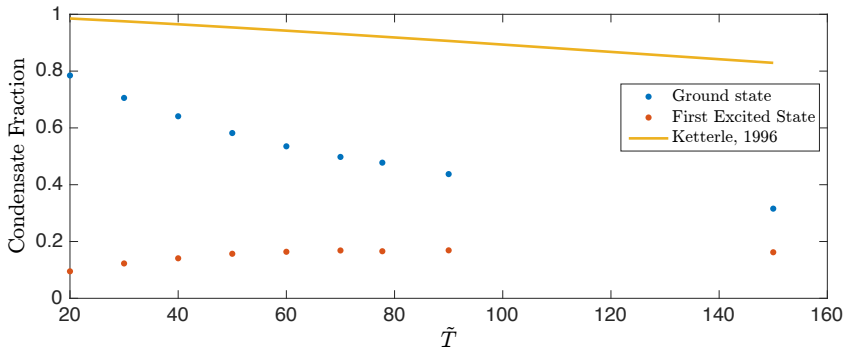

Figure 6.5: The fraction of component 1 in the ground (condensate) state and the first excited state as a function of temperature, for the ^{87}Rb simulations, compared with the condensate fraction from Equation 4.15[17].

It is interesting to note that although the damping coefficient is very different at high temperatures, the two-time correlation functions for the centre of mass are still well described by the analytic forms, but with a different choice for the damping coefficient. This implies that the centre of mass of the system can still be thought of as a damped harmonic oscillator subject to a random driving force, which is what would be expected from the Kohn Theorem.

Equipartition Theorem

The analytic results predicted that $g_X(0) = \frac{\bar{T}_{CM}}{\Omega^2}$ and $g_V(0) = \bar{T}_{CM}$, which in turn can be used to calculate the potential and kinetic energy and show that the equipartition theorem is satisfied, Section 5.4. Values of $\tilde{\bar{T}}_{CM}$ using Equation 5.45, $g_X(0)$ and $g_V(0)$ were plotted against $\tilde{T}$ in Figure 6.6a. Although there is slight deviation for higher temperature due to higher temperature fluctuations requiring larger ensembles, there is still good agreement for both the values for $\tilde{\bar{T}}_{CM}$ found using the position and velocity two-time correlation functions.

Even better agreement is observed calculating the energy of the centre of mass explicitly,

$$\tilde{E}_{COM} = \widetilde{PE} + \widetilde{XE} \tag{6.24}$$

$$= \frac{1}{2}\left(g_X(0) + g_V(0)\right). \tag{6.25}$$

The energy of the centre of mass shows very good agreement with the analytic predictions, even at high temperature when the wavefunction has very little Thomas Fermi character (Figure 6.6b).

The equipartition continues to hold even in the high temperature regime because the condensate is in a harmonic trap, and the centre of mass has two degrees of freedom, regardless of the temperature.

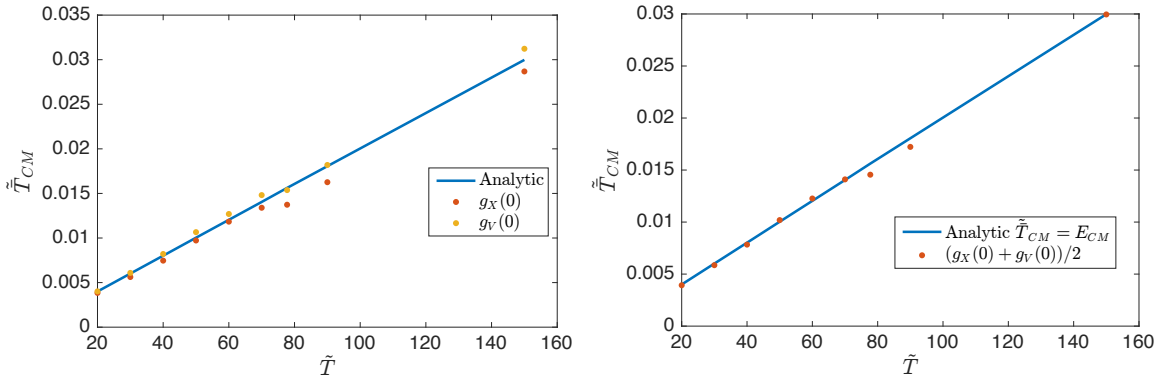

(a) **(b)**

Figure 6.6: (a)$\tilde{\tilde{T}}_{CM}$ against $\tilde{T}$. The blue line is obtained from Equation 5.45, the red points from $g_X(0)$ and the yellow points from $g_V(0)$. (b)The energy of the centre of mass in dimensionless units, $\tilde{E}_{CM}$, plotted against temperature. The analytic result is given by the blue line and the red points are values obtained from the two-time correlation functions.

The equipartition theorem only holds in equilibrium, and so the systems must be allowed to thermalise before using the values of the position and velocity of the centre of mass. Using the values of the two-time correlation functions at $\tau = 0$ is sufficient because the two-time correlation functions were calculated using data from the thermalised system. The effect of thermalisation on the energy of the centre of mass for an initially Thomas Fermi State is demonstrated in Figure 6.7a. The system starts out in a Thomas-Fermi State where the centre of mass has no energy, and on average gains energy due to thermal noise during the first damping time as the system thermalises. The damping rate has no effect on the energy of centre of mass of the thermalised system, but does affect the time for thermalisation.

It is also interesting to investigate the total energy of the condensate, as it evolves in time from an initially Thomas-Fermi state. The total energy of the condensate is found by evaluating the kinetic and potential energy of the condensate in the harmonic oscillator basis, and using a Gauss-Hermite quadrature method to evaluate the interaction energy in the position basis. We can see in Figure 6.7b that the total energy seems to reach equilibrium much faster than when considering just the centre of mass of the system.

6.2.3 ^{23}Na Condensate Simulations

For the simulations of a condensate of ^{23}Na in a thermal cloud of ^{87}Rb, a similar approach was taken to the simulations with a ^{87}Rb condensate. For simulations at different temperatures, the transverse trapping frequency of the thermal cloud was varied, while the other trapping frequencies for each component were held constant. This allowed the damping coefficient to be tuned to give numerically expedient simulations. The constant trapping frequencies were $\Omega = 94.2$ Hz, $\omega_{\perp,1} = 4400$ Hz, $\omega_{x,2} = 84.8$ Hz. The component populations were $N_1 = 10^5$ and $N_2 = 10^6$. The ^{23}Na-^{23}Na s-wave scattering length is

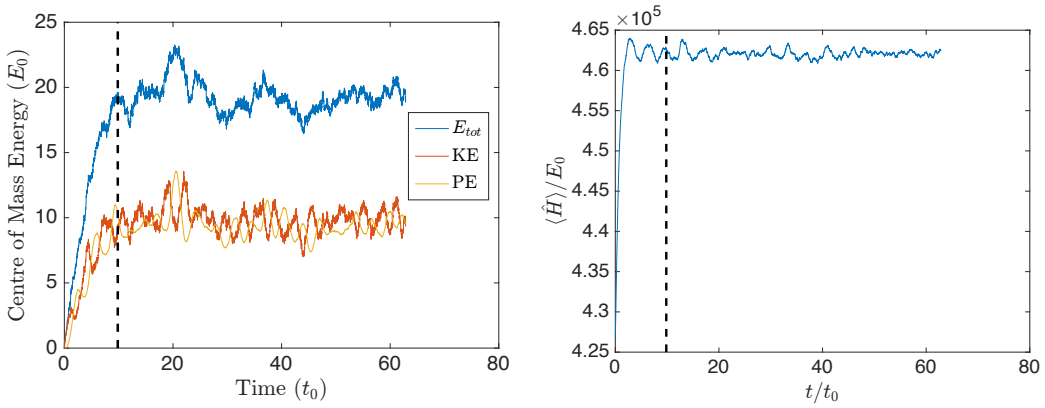

(a) **(b)**

Figure 6.7: (a) The kinetic, potential, and total energy for a condensate centre of mass of ^{87}Rb at $\tilde{T} = 20$ with parameters described in Section 6.2.2 and Table 6.1, with an ensemble of 300 elements. The black dashed line shows one damping time of the system. The system was initially in a Thomas-Fermi State. (b) The total energy for a condensate of ^{87}Rb at $\tilde{T} = 20$ with parameters described in Section 6.2.2 and Table 6.1, using an ensemble of 240 elements. The black dashed line shows one damping time of the centre of mass of the system. The system was initially in a Thomas-Fermi State.

$\tilde{T}$	T (nk)	$\omega_{\perp,2}$ (Hz)	$\tilde{\mu}_2$	$\tilde{\mathcal{M}}$	$\tilde{\Gamma}$	$\tilde{\tilde{T}}_{CM}$
20	14.4	9.74	-0.0187	0.0102	0.114	0.002
30	21.6	17.9	-0.0309	0.00925	0.104	0.003
40	28.8	27.5	-0.0321	0.0119	0.133	0.004
45	32.4	32.9	-0.0358	0.0120	0.134	0.0045
50	36.0	38.5	-0.0522	0.00912	0.102	0.005
75	54.0	70.7	-0.0720	0.00992	0.111	0.0075
150	108	200	-0.111	0.0129	0.144	0.015
500	360	1220	-0.527	0.00904	0.101	0.05

Table 6.2: Variable parameters for SPGPE simulations of a psuedo-1D condensate of ^{23}Na in a thermal cloud of ^{87}Rb .

$a_s = a_{11} = 63a_0$ and so the dimensionless non-linear interaction coefficient for these simulations is $\tilde{g} = 0.0575$ and the dimensionless chemical potential of component 1 which is assumed to be Thomas-Fermi is $\tilde{\mu}_1 = 45.3$. The scattering length for interactions between the ^{23}Na condensate and ^{87}Rb thermal cloud is $a_{12} = 104a_0$. For the different temperature simulations $\omega_{\perp,2}$ was varied which effected the other simulation parameters, as show in Table 6.2.

For these simulations, although the proper form of $\mathcal{M}$ is not known, we expect that the form given by Equation 4.7 will give a reasonably accurate approximation. Even if the value of $\mathcal{M}$ differs from the physical result, we still expect our simulations to be consistent with analytic forms, because the simulations are using $\mathcal{M}$ as a parameter.

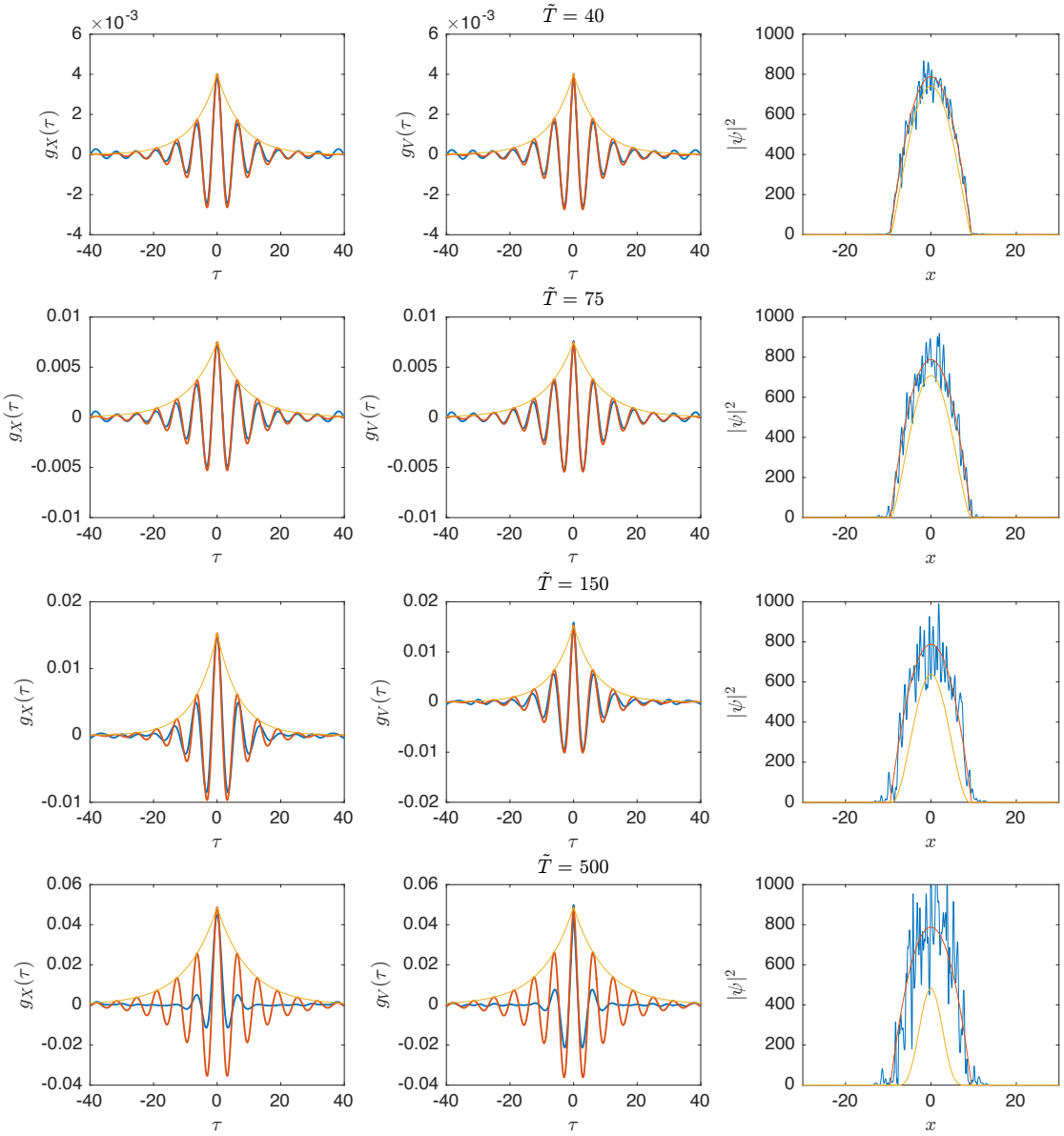

Figure 6.8: Plots of two-time correlation functions versus time, for a condensate of ^{23}Na over a range of temperatures $\tilde{T} = 40, 75, 150, 500$; also shown are condensate densities (right column). The analytic forms for $g_X(\tau)$ (5.80) and $g_V(\tau)$ (5.93) are plotted in the first and second column (orange) together with the results from the SPGPE simulations (blue), and the analytic decay envelope, (5.95) (yellow). In the third column we plot the particle densities for the zero-temperature Thomas-Fermi solution (2.9) (red), the condensate orbital obtained using the Penrose-Onsager criterion (6.22, 6.23), and a particular SPGPE trajectory (blue). τ is in units of $1/\Omega$, x is in units of $a_{x,1}$.

As with the ^{87}Rb simulations, the ^{23}Na simulations were performed using a semi-implicit Euler method, calculating the state of the wavefunction every 0.0314 t_0 from $t = 0t_0$ to

$t = 3000\ t_0$. The damping times were tuned to be approximately $1/\tilde{\Gamma} = 10$, and as with the ^{87}Rb simulations the long trajectories were divided into smaller trajectories that ran for 50 t_0, as well as discounting the first trajectory in each run. By running 6 simulations in parallel, 366 trajectories were found for each set of parameters. Because of the different a_{11} for the ^{23}Na atoms the chemical potential was able to be chosen much lower, allowing a lower energy cutoff. Because fewer energy modes were considered, this meant that more trajectories were able to be found numerically for a similar time of simulation compared to the ^{87}Rb simulations.

The values of position and velocity at all of the timesteps for the different trajectories were used to construct two-time correlation functions for position and velocity, some of these are shown for different temperatures in Figure 6.8.

Interestingly the analytic forms of the two-time correlation function hold even as the temperature becomes greater than the chemical potential. At these temperatures the condensate fraction density given by the Penrose-Onsager criterion is still a close match for the Thomas-Fermi state. This may be because the component 1 of the ^{23}Na simulations has approximately double the number of particles, allowing it to remain Thomas-Fermi at higher temperatures.

Although there is good agreement between the analytic and simulated two-time correlation functions, the relative error in the damping coefficient does still increase with temperature as the condensate fraction loses Thomas-Fermi character and becomes better described as a Gaussian, Figure 6.9.

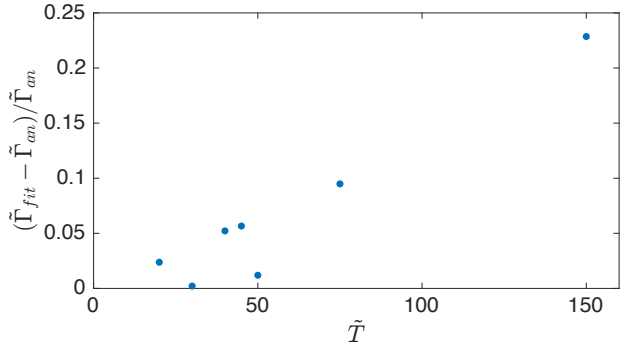

Figure 6.9: The relative error in the dimensionless damping coefficient for different system temperatures, for the ^{23}Na simulations. Although the relative error is small, it does on average increase with temperature, especially for $\tilde{T} > \tilde{\mu}_1$.

A large point of difference between the simulations using a component 1 of ^{87}Rb and a component 1 of ^{23}Na is the difference in the interaction strength, characterised by $\tilde{g}$. $\tilde{g}$ is about larger by a factor of around 4.5 for the ^{87}Rb simulations, compared with the ^{23}Na simulations. There is also a large difference in $\tilde{\mu}_1$, which is almost twice as large in the ^{87}Rb simulations. The lower interaction strength and chemical potential may effect the interactions between the non-condensate and condensate regions of component 1, allowing it to remain Thomas-Fermi for higher temperatures.

Chapter 7

Conclusion

In this project we have investigated the centre of mass motion of an elongated harmonically trapped BEC in a cloud of distinct atoms. **C**-field techniques were applied, allowing us to treat the low energy modes containing the condensate as a coherent region (**C** region), and the thermal cloud as an incoherent region (**I** region), acting as a thermal reservoir. Because the two regions are composed of quantum mechanically distinguishable particles from each other, particle exchange is forbidden, and we can ignore the number damping term in the SPGPE, giving us the energy-damped SPGPE (Equation 4.3).

The physical validity regime was investigated, to ensure we could find physically realistic parameters where the 1D model is valid. The system had to be in the correct temperature regime with component 1 having a significant condensate fraction, and component 2 entirely thermalised. There were strict requirements for the trapping geometry of component 1, ensuring that there were no transverse oscillations, which allows us to treat it as pseudo 1D. However the confining potential cannot be so tight that the scattering interactions within the condensate are no longer three dimensional. The trap geometry for the thermal cloud is not as constrained, and so this gives us freedom to vary other parameters by changing the component 2 trapping frequencies. The number of particles in each component is conserved, which sets the chemical potentials. All of the parameters are chosen to be in a range that is physically realisable

Following from the work of [6] and [5], under the assumption that the wavefunction remained in a Thomas-Fermi state, an analytic form was obtained for the equation of motion for the centre of mass of the condensate. This equation of motion had the form of a damped simple harmonic oscillator subject to a random driving force. Analytic expressions for the damping and noise were found in terms of the system parameters.

Following and extending on the derivation found in [19], the two-time correlation functions for both position and velocity for a simple harmonic oscillator with a random driving force. These analytic two-time correlation functions were found to be consistent with the equipartition theorem. These analytic two-time correlation results were validated by numerically simulating a damped harmonic oscillator driven by a random force, giving almost exact agreement.

The central aim of this work has been to compare the analytic results with simulations using the full SPGPE.

Two different physical regimes were simulated over a range of temperatures; one with a condensate of ^{87}Rb and a thermal cloud of ^{87}Rb, and one with a condensate of ^{23}Na and a thermal cloud of ^{87}Rb. For the ^{87}Rb-^{87}Rb simulations we assume that the two regions are in different internal state. It is important to note that for the ^{23}Na-^{87}Rb simulations there is likely a missing factor in the energy damping rate due to the mass difference, which would be interesting to explore in future work. For these simulations, many trajectories were performed, and the position and velocity of the centre of mass of the $\mathbf{C}$ field region was found. Using the values of position and velocity for the centre of mass of the condensate, two-time correlation functions were numerically computed. For low temperature, these showed excellent agreement with the analytic forms of the two-time correlation functions using analytically derived equations for the damping coefficient and the effective centre of mass temperature.

For higher temperatures, as the condensate becomes less well described by the Thomas-Fermi state, the two-time correlation functions become less well described by the analytic forms, as is expected. This departure from Thomas-Fermi behaviour was investigated using the Penrose-Onsager criterion.

Surprisingly, the ^{23}Na-^{87}Rb simulations give good agreement with the analytic two-time correlation functions, for temperatures much higher than the chemical potential. This may be caused by the lower interaction strength of ^{23}Na, meaning that the non-condensate fraction does not interact as strongly with the condensate.

This project is a rare case where the full SPGPE can be solved almost exactly, and this is backed up by the excellent agreement between our analytic and numerical results. Because care has been taken to ensure that the parameters chosen were experimental realistic, the results of this work may be experimentally testable.

Appendix A

Integral from Section 5.1.2

Here we compute the integral

$$K = \int dk\ S_1(k)\ k^2 \left[\left(\int dx\ n_{TF}(x,t)\, \mathrm{e}^{ikx} \right) \left(\int dx'\ n_{TF}(x',t)\, \mathrm{e}^{-ikx'} \right) \right] \tag{A.1}$$

The integral over x can be interpreted as the Fourier transform of the Thomas-Fermi density.

$$\begin{aligned}
\int_{-\infty}^{\infty} dx\ n_{TF}(x,t)\, \mathrm{e}^{ikx} &= \int_{X-R}^{X+R} dx\ n_{TF}(x,t)\, \mathrm{e}^{ikx} && \text{(A.2)} \\
&= \int_{X-R}^{X+R} dx\ n_0 \left(1 - \frac{(x - X(t))^2}{R^2} \right) \mathrm{e}^{ikx} && \text{(A.3)} \\
&= \int_{-R}^{R} dx\ n_0 \left(1 - \frac{x^2}{R^2} \right) \mathrm{e}^{ik(x+X)} && \text{(A.4)} \\
&= \left[\frac{n_0}{ik}\, \mathrm{e}^{ik(x+X)} \right]_{-R}^{R} - \int_{-R}^{R} dx\ n_0 \frac{x^2}{R^2}\, \mathrm{e}^{ik(x+X)}\,. && \text{(A.5)}
\end{aligned}$$

Using integration by parts on the second term, we obtain

$$\begin{aligned}
\int_{-\infty}^{\infty} dx\ n_{TF}(x,t)\, \mathrm{e}^{ikx} &= \left[\frac{n_0}{ik}\, \mathrm{e}^{ik(x+X)} \right]_{-R}^{R} - \frac{n_0}{R^2} \left[\left(\frac{x^2}{ik} - \frac{2x}{k^2} - \frac{2}{ik^3} \right) \mathrm{e}^{ik(x+X)} \right]_{-R}^{R} && \text{(A.6)} \\
&= n_0 \left(\frac{4}{R\ k^2} \cos(kR) - \frac{4}{R^2 k^3} \sin(kR) \right) \mathrm{e}^{ikX}\,. && \text{(A.7)}
\end{aligned}$$

The integral over x' will be equal to the complex conjugate of Equation A.7, hence the integral becomes

$$K = \int_{-\infty}^{\infty} dk\ S_1(k)\ k^2 \left| \int dx\ n_{TF}(x,t)\, \mathrm{e}^{ikx} \right|^2 \tag{A.8}$$

$$= \int_{-\infty}^{\infty} dk\ S_1(k)\ k^2 n_0^2 16 \left(\frac{\cos(kR)}{R\ k^2} - \frac{\sin(kR)}{R^2 k^3} \right)^2 \tag{A.9}$$

$$= 32 n_0^2 \int_0^{\infty} dk\ S_1(k)\ k^2\ R^2 \left(\frac{\cos(kR)}{(kR)^2} - \frac{\sin(kR)}{(kR)^3} \right)^2 . \tag{A.10}$$

Thus using the definition of $S_1(k)$

$$S_1(k) = \frac{1}{\sqrt{8\pi a_\perp^2}} \operatorname{erfcx}\left(\frac{|k| a_\perp}{\sqrt{2}} \right) \tag{A.11}$$

and defining the dimensionless variable $z = kR$, this integral can be written in the form

$$K = \frac{32 n_0^2}{R\sqrt{8\pi a_\perp^2}} \int_0^{\infty} dz \operatorname{erfcx}\left(\frac{\lambda z}{\sqrt{2}} \right)\ z^2 \left(\frac{\cos(z)}{z^2} - \frac{\sin(z)}{z^3} \right)^2 \tag{A.12}$$

where

$$\lambda = a_\perp / R. \tag{A.13}$$

Bibliography

[1] M. H. Anderson, J. R. Ensher, M. R. Matthews, C. E. Wieman, and E. A. Cornell, Observation of Bose-Einstein condensation in a dilute atomic vapor, *Science* **269**(5221), 198 (1995).

[2] F. Dalfovo, S. Giorgini, L. P. Pitaevskii, and S. Stringari, Theory of Bose-Einstein condensation in trapped gases, *Reviews of Modern Physics* **71**(3), 463 (1999).

[3] C. W. Gardiner and M. J. Davis, The stochastic Gross-Pitaevskii equation II, *Journal of Physics B: Atomic, Molecular and Optical Physics* **36**(23), 4731–4753 (2003).

[4] G. Modugno, Bose-einstein condensation of potassium atoms by sympathetic cooling, *Science* **294**(5545), 1320–1322 (2001).

[5] Z. Atayee, Kohn Mode Damping in Bose-Einstein Condensate, *Hons Dissertation, Otago*, (2016).

[6] R. G. McDonald and A. S. Bradley, Brownian motion of a matter-wave bright soliton moving through a thermal cloud of distinct atoms, *Physical Review A* **93**, 063604 (2016).

[7] W. Kohn, Cyclotron resonance and de haas-van alphen oscillations of an interacting electron gas, *Physical Review* **123**(4), 1242–1244 (1961).

[8] J. F. Dobson, Harmonic-potential theorem: implications for approximate many-body theories, *Physical Review Letters* **73**(16), 2244 (1994).

[9] P. B. Blakie, A. S. Bradley, M. J. Davis, R. J. Ballagh, and C. W. Gardiner, Dynamics and statistical mechanics of ultra-cold Bose gases using c-field techniques, *Advances in Physics* **57**(5), 363–455 (2008).

[10] R. G. McDonald, C-Field Dynamics in 1D Bose Gases, *MSc Thesis, Otago*, (2015).

[11] S. J. Rooney, Single Vortex Dynamics in High Temperature Bose-Einstein Condensates, *Hons Dissertation, Otago*, (2009).

[12] C. Gardiner and P. Zoller, *Quantum Noise: A Handbook of Markovian and Non-Markovian Quantum Stochastic Methods with Applications to Quantum Optics* (Springer, Berlin, Heidelberg, 2004).

[13] C. W. Gardiner, *Stochastic methods : a handbook for the natural and social sciences* (Springer, Berlin, Heidelberg, 2009).

[14] C. N. Weiler, T. W. Neely, D. R. Scherer, A. S. Bradley, M. J. Davis, and B. P. Anderson, Spontaneous vortices in the formation of boseeinstein condensates, *Nature* **455**(7215), 948–951 (2008).

[15] S. J. Rooney, T. W. Neely, B. P. Anderson, and A. S. Bradley, Persistent-current formation in a high-temperature bose-einstein condensate: An experimental test for classical-field theory, *Physical Review A* **88**(6), (2013).

[16] A. S. Bradley, S. J. Rooney, and R. G. McDonald, Low-dimensional stochastic projected Gross-Pitaevskii equation, *Physical Review A* **92**(3), (2015).

[17] W. Ketterle and N. J. Van Druten, Bose-Einstein condensation of a finite number of particles trapped in one or three dimensions, *Physical Review A* **54**(1), 656 (1996).

[18] A. S. Bradley and P. B. Blakie, Stochastic projected Gross-Pitaevskii equation for spinor and multicomponent condensates, *Physical Review A* **90**, 023631 (2014).

[19] G. K. Batchelor, *The Theory of Homogeneous Turbulence* (Cambridge University Press, Cambridge, UK, 1953).

[20] R. Gerritsma, S. Whitlock, T. Fernholz, H. Schlatter, J. A. Luigjes, J.-U. Thiele, J. B. Goedkoop, and R. J. C. Spreeuw, Lattice of microtraps for ultracold atoms based on patterned magnetic films, *Physical Review A* **76**, 033408 (2007).

[21] A. Görlitz, J. M. Vogels, A. E. Leanhardt, C. Raman, T. L. Gustavson, J. R. Abo-Shaeer, A. P. Chikkatur, S. Gupta, S. Inouye, T. Rosenband, and W. Ketterle, Realization of Bose-Einstein Condensates in Lower Dimensions, *Physical Review Letters* **87**, 130402 (2001).

[22] M. Mudrich, S. Kraft, K. Singer, R. Grimm, A. Mosk, and M. Weidemüller, Sympathetic Cooling with Two Atomic Species in an Optical Trap, *Physical Review Letters* **88**, 253001 (2002).

[23] H. Ott, J. Fortagh, G. Schlotterbeck, A. Grossmann, and C. Zimmermann, Bose-einstein condensation in a surface microtrap, *Physical Review Letters* **87**(23), (2001).

[24] S. J. Rooney, P. B. Blakie, and A. S. Bradley, Numerical method for the stochastic projected Gross-Pitaevskii equation, *Physical Review E* **89**, 013302 (2014).